https://doi.org/10.5194/bg-2021-122
Preprint. Discussion started: 17 May 2021
© Author(s) 2021. CC BY 4.0 License.

Biogeosciences Discussions
Open Access
EGU

Summertime productivity and carbon export potential in the Weddell Sea, with a focus on the waters adjacent to Larsen C Ice Shelf

Raquel F. Flynn[1*], Thomas G. Bornman[2,3], Jessica M. Burger[1], Shantelle Smith[1], Kurt A.M. Spence[1] and Sarah E. Fawcett[1,4]

[1]Department of Oceanography, University of Cape Town, Cape Town, South Africa
[2]South African Environmental Observation Network, Elwandle Coastal Node, Port Elizabeth, South Africa
[3]Institute for Coastal and Marine Research, Nelson Mandela University, Port Elizabeth, South Africa
[4]Marine and Antarctic Research centre for Innovation and Sustainability (MARIS), University of Cape Town, Cape Town, South Africa

[*]*Correspondence to*: Raquel F. Flynn (flyraq001@myuct.ac.za)

Abstract

The Weddell Sea (WS) represents a point of origin in the Southern Ocean where globally-important water masses form. Biological activities in WS surface waters thus affect large-scale ocean biogeochemistry. During summer 2018/2019, we measured net primary production (NPP), nitrogen (nitrate, ammonium, urea) uptake, and nitrification in the western WS at the Antarctic Peninsula (AP) and Larsen C Ice Shelf (LCIS), in the southwestern Weddell Gyre (WG), and at Fimbul Ice Shelf (FIS) in the south-eastern WS. The highest average rates of NPP and greatest nutrient drawdown occurred at LCIS. Here, the phytoplankton community was dominated by colonial *Phaeocystis antarctica*, with diatoms increasing in abundance later in the season as sea-ice melt increased. At the other stations, NPP was variable, and diatoms known to enhance carbon export (e.g., *Thalassiosira* spp.) were dominant. Euphotic zone nitrification was always below detection, such that nitrate uptake could be used as a proxy for carbon export potential, which was highest in absolute terms at LCIS and the AP. Surprisingly, the highest f-ratios occurred near FIS rather than LCIS (average of 0.73 ± 0.09 versus 0.47 ± 0.08). We attribute this to partial ammonium inhibition of nitrate uptake at LCIS (where ammonium concentrations were 0.6 ± 0.4 µM, versus 0.05 ± 0.1 µM at FIS) driven by increased heterotrophy following the accumulation of nitrate-fuelled phytoplankton biomass in early summer. Across the WS, carbon export appears to be driven by a combination of physical, chemical, and biological factors, with the highest export flux occurring at the ice shelves and lowest in the central WG.

Keywords: Nitrogen uptake, primary production, phytoplankton taxonomy, nutrient depletion, ammonium inhibition, Antarctic ice shelves

https://doi.org/10.5194/bg-2021-122
Preprint. Discussion started: 17 May 2021
© Author(s) 2021. CC BY 4.0 License.

1. Introduction

The Southern Ocean is an important driver of Earth's climate as it transports large quantities of heat and dissolved gases, and supplies 65-85% of the global ocean's nutrients (Keffer and Holloway 1988; Sarmiento et al. 2004; Frölicher et al. 2015; Keller et al. 2016). Despite the Southern Ocean's central role in atmospheric CO_2 removal (DeVries 2014; Frölicher et al. 2015; Gruber et al. 2019), the incomplete drawdown of nutrients (i.e., nitrate, phosphate, and silicic acid) in its surface waters due to iron and light limitation of phytoplankton (Martin et al. 1991; Sunda and Huntsman 1997) represents a missed opportunity for CO_2 removal (Sarmiento and Toggweiler 1984). The Weddell Sea constitutes a point of origin in the Southern Ocean where water masses form and communicate with the atmosphere before subducting (Muench and Gordon 1995; Talley et al. 2011), thereby setting the initial physical and chemical conditions of the deep global ocean. Biogeochemical cycling in the surface Weddell Sea thus has implications for carbon transfer to and storage within the ocean interior (Hoppema et al. 2004; Kerr et al. 2018). The southern and western Weddell Sea are bounded by ice shelves, which promote high rates of summertime productivity, nutrient drawdown and carbon export (El-Sayed and Taguchi 1981; Hoppema and Goeyens 1999; Hoppema et al. 2000) largely because the surface ecosystem is less iron- and light-limited in the ice shelf-adjacent waters than in open waters (Klunder et al. 2014).

The Weddell Sea is separated from the Antarctic Circumpolar Current (ACC) and open Southern Ocean by the Weddell Sea fronts (Orsi et al. 1995). The general large-scale circulation takes the form of a cyclonic, wind-driven and topographically-steered gyre, the Weddell Gyre (WG) (Fahrbach et al. 1994, 1995; Orsi et al.1995), that transports the relatively warm, saline waters of the ACC into the polar region where they are cooled and become more saline (Huhn et al. 2008; Nicholls et al. 2009; van Caspel et al. 2015). The production of dense bottom water is thought to occur at two sites in the Weddell Sea: at Filchner-Ronne Ice Shelf (FRIS) and Larsen C Ice Shelf (LCIS) (Gordon et al. 1993; Schröder et al. 2002; Schodlok et al. 2002). Here, Modified Warm Deep Water (MWDW) intrudes onto the continental shelf and mixes with Antarctic Surface Water (ASW). ASW is cooled to freezing point through heat loss to the atmosphere, as well as being supercooled under the ice shelves, and increases in salinity due to brine rejection during sea-ice formation, which further increases its density (Brennecke 1921; Mosby 1934; Gill 1973). As MWDW flows throughout the WG, its physical and chemical properties are altered due to mixing with ASW, ultimately resulting in the formation of dense bottom waters. Upon reaching the Antarctic Peninsula (AP), the transformed bottom waters either spill out over the shelf and re-enter the ACC or are entrained into the eastward flowing limb of the WG (Orsi et al. 1993; Locarnini et al. 1993).

Weddell Sea surface waters are warm and saline while those over the continental shelf are relatively cool and fresh (Nicholls et al. 2004). These different waters are separated by the Antarctic Slope Front (ASF; Jacobs 1986; 1991), a fast-flowing jet situated between the 500 m and 1000 m isobath that separates the Open Ocean Zone (OOZ) from the Coastal and Continental Shelf Zone (CCSZ; Jacobs 1986; 1991; Muench and Gordon 1995). The Antarctic CCSZ has been observed to host high rates of productivity in the summer (e.g., Smith and Nelson 1990; Arrigo et al. 2008) as melting sea-ice supplies dissolved iron and increases water column stratification, yielding ideal conditions for phytoplankton growth (Lannuzel et al. 2008). Inputs of dissolved iron from continental shelf sediments and coastal runoff further elevate the ambient iron concentrations, such that the CCSZ seldom experiences iron-depletion (Klunder et al. 2014). As a result, the large phytoplankton blooms of the CCSZ can at

https://doi.org/10.5194/bg-2021-122
Preprint. Discussion started: 17 May 2021
© Author(s) 2021. CC BY 4.0 License.

times almost completely deplete surface nitrate concentrations (Jennings et al. 1984; Hoppema et al. 2000; Henley et al. 2017), supporting high rates of carbon export (Arrigo et al. 2008). In contrast, the OOZ is far less productive due to deeper mixed layer depths (MLD) that lead to light limitation of phytoplankton, along with persistent iron-deplete conditions (Klunder et al. 2011; De Jong et al. 2012). Here, surface nutrients are never fully consumed and carbon export rates are low (Boyd et al. 2008; Boyd and Ellwood 2010; Klunder et al. 2011; De Jong et al. 2012).

On an annual basis, phytoplankton growth in the euphotic zone that is fuelled by nitrate supplied from below (i.e., "new production") must be balanced by the export of sinking organic matter into the ocean interior (i.e., "export production"), thus driving CO_2 removal (Dugdale and Goering 1967; Eppley and Peterson 1979). By contrast, phytoplankton growth supported by nitrogen (N) sources that are recycled in the euphotic zone, such as ammonium and urea (i.e., "regenerated production"), results in no net removal of CO_2 to the deep ocean. The biologically-driven flux of carbon from surface waters, termed the "biological pump", transfers CO_2 to the isolated waters of the deep ocean, maintaining the atmospheric concentration of this greenhouse gas (Volk and Hoffert 1985). The high nutrient-low chlorophyll state of much of the Southern Ocean represents a "leak" in the ocean's biological pump since by consuming mixed-layer nutrients more completely, phytoplankton could theoretically lower atmospheric CO_2 (Sarmiento and Toggweiler 1984). Indeed, a leading hypothesis for the 80-100 ppm decrease in atmospheric CO_2 that characterized the ice ages is more complete consumption of surface nutrients (i.e., a more efficient biological pump) in the open Southern Ocean (Sigman and Boyle 2000; Sigman et al. 2010; Martínez-García et al. 2014).

Since phytoplankton in the CCSZ of the Weddell Sea consume much of the nitrate supplied to the surface (Jennings et al. 1984; Hoppema et al. 2000), they should, by mass balance, drive the export of a significant amount of atmospheric CO_2 to depth, most of which will be subducted in newly-formed bottom waters to be sequestered for >1000 years (Ito et al. 2010). Understanding the controls on biological nutrient utilization in the Weddell Sea, particularly the CCSZ, is thus central to our understanding of its contribution to the Southern Ocean's role in setting atmospheric CO_2. In general, phytoplankton growth in the Weddell Sea is regulated by the seasonal cycle of sea-ice, with the associated availability of light and iron imposing the main constraints (El-Sayed and Taguchi 1981). In winter, sea-ice formation and wind-driven mixing supply high concentrations of nutrients to ASW (Hoppema et al. 2007; 2015) that remain largely unconsumed due to the deep mixed layers and short days (Cota et al. 1992; Scharek et al. 1994; Spiridonov et al. 1996). Relief from light limitation in spring and early summer driven by increased water-column stratification from sea-ice melt combined with enhanced solar radiation leads to the development of phytoplankton blooms. The size and duration of these blooms is ultimately dependent on both macro- (e.g., nitrate and silicate) and micronutrient (e.g., iron) availability (Martin et al. 1991; Boyd 2004; Boyd and Ellwood 2010; Llort et al. 2015).

Observations suggest that Weddell Sea phytoplankton blooms are initially dominated by smaller phytoplankton (e.g., *Phaeocystis antarctica*; 2-6 μm) that are well-adapted to the low light conditions associated with the fairly deep springtime mixed layers (Schoemann et al. 2005). The ability of these smaller cells to rapidly grow and consume the available nutrients results in bloom initiation. However, their small size also means that *P. antarctica*

https://doi.org/10.5194/bg-2021-122
Preprint. Discussion started: 17 May 2021
© Author(s) 2021. CC BY 4.0 License.

experience high rates of predation by microzooplankton and sink fairly slowly, which enhances their contribution to the microbial loop and decreases their carbon export potential (Hansen et al. 1994; 1997). As the season progresses, rising air temperatures leads to increased sea-ice melt and warmer sea surface temperatures (SST), resulting in an increasingly stratified upper water column that provides optimal conditions for the growth of larger phytoplankton such as diatoms (Goffart et al. 2000; Nissen and Vogt 2020). Diatoms tend to rely heavily on nitrate as their dominant N source (Malone 1980; Lomas and Glibert 1999; Fawcett and Ward 2011; Glibert et al. 2016) and are a major vector for carbon export in the Southern Ocean due to their rapid sinking rates that are facilitated by biogenic silica ballasting (Tréguer et al. 2017). The seasonal shift in the Weddell Sea community from small, non-silicified phytoplankton to larger, more heavily-silicified species is thus associated with a significant increase in carbon export (Treguer and Jacques 1992; De Baar et al. 2005; Boyd et al. 2007). Sea-ice melt also supplies high concentrations of dissolved iron to surface waters (up to 7 nM in the western Weddell Sea; Lannuzel et al. 2008; Klunder et al. 2014), alleviating phytoplankton from iron limitation and supporting a high degree of surface nitrate drawdown (Klunder et al. 2011, 2014). Eventually, as surface iron (and occasionally, nitrate; Hoppema, et al., 2000) concentrations again become limiting, phytoplankton rely proportionally more on ammonium and other regenerated N sources that have become increasingly available due to heterotrophic processing of the accumulated (i.e., bloom) biomass (Goeyens et al. 1995; Semeneh et al. 1998). The phytoplankton community consequently shifts once more towards smaller species that are better adapted to low iron conditions and specialize in the consumption of regenerated N, ultimately leading to a decrease in carbon export (Goeyens et al. 1995).

The Weddell Sea is particularly understudied near LCIS where thick sea-ice conditions persist year-round. To our knowledge, the only biogeochemical study conducted in the vicinity of LCIS was undertaken in the austral summer of 1992/3. Using measurements of nutrient depletion, Hoppema et al. (2000) estimated primary production in the vicinity of LCIS to be 47.5-95 mmol C m^{-2} d^{-1}, while in the central Weddell Sea it was substantially lower at 8.3 mmol C m^{-2} d^{-1}. However, the study did not characterize the phytoplankton community, so the extent to which phytoplankton diversity may have influenced primary production and nutrient drawdown cannot be surmised. To evaluate the summertime fertility of the Weddell Sea and the potential importance of different phytoplankton groups for carbon production and export, we directly measured the rates of total, new, and regenerated production in the western Weddell Sea (predominantly at LCIS), as well as at Fimbul Ice Shelf (FIS) in the south-eastern Weddell Sea. Rates of nitrification were also quantified to account for any nitrate regenerated within the euphotic zone at the time of sampling as this N flux supports regenerated rather than new production (e.g., Yool et al. 2007; Peng et al. 2018; Mdutyana et al. 2020). We interpret our rate data in the context of concurrent measurements of regional hydrography, macronutrient concentrations and ratios, and phytoplankton community composition.

2. Methods

2.1. Field collections

Sampling was conducted in the austral summer of 2018/2019 during the Weddell Sea Expedition onboard the R/V *SA Agulhas II*. A total of 19 stations were sampled across the Weddell Sea and are categorised based on their geographic position as Antarctic Peninsula (AP), Larsen C Ice Shelf (LCIS), Weddell Gyre (WG), or Fimbul Ice Shelf (FIS) stations (Table 1; Figure 1). Hydrographic data were collected using a Seabird conductivity-

https://doi.org/10.5194/bg-2021-122
Preprint. Discussion started: 17 May 2021
© Author(s) 2021. CC BY 4.0 License.

159 temperature-depth (CTD) profiler equipped with a photosynthetically active radiation (PAR) sensor. Density
160 (sigma-theta; σ_θ) was derived from CTD measurements of temperature, salinity and pressure, and was used to
161 identify the water masses present. At all stations, the mixed layer depth (MLD) was determined as the depth at
162 which the Brunt-Väisälä frequency squared (N^2; a function of σ_θ) reached a maximum (Schofield et al. 2015;
163 Carvalho et al. 2017).
164

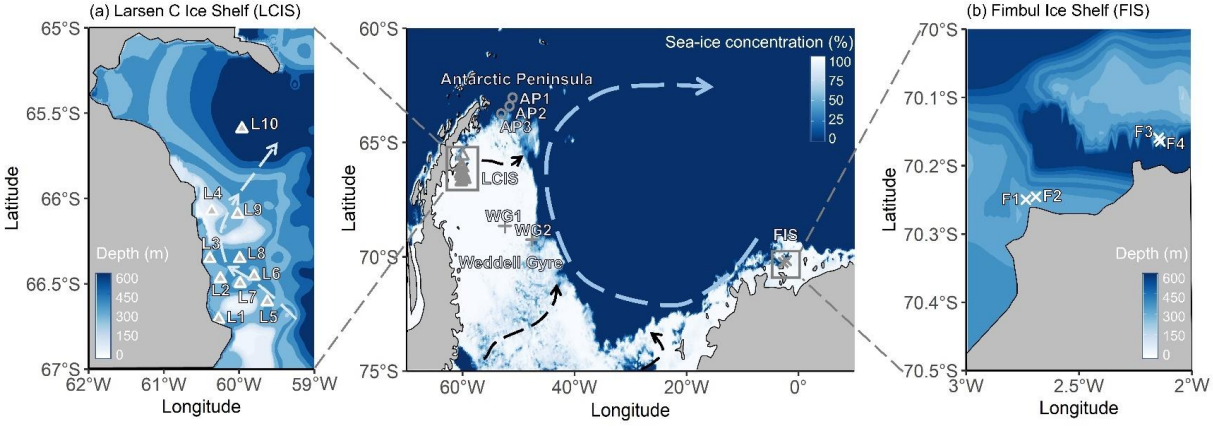

165 **Figure 1.** Maps of the Weddell Sea, Larsen C Ice Shelf (LCIS; insert a) and Fimbul Ice Shelf (FIS; insert b)
166 showing the position of the stations where rate experiments were conducted during the Weddell Sea Expedition
167 in January/February 2019. The symbols represent the different regions of the Weddell Sea sampled during the
168 expedition (circle – Antarctic Peninsula (AP); cross – FIS; triangle – LCIS; plus sign – Weddell Gyre (WG)). The
169 general cyclonic circulation of the Weddell Gyre (dashed blue arrow) is illustrated on the central map, and the
170 dashed black arrows indicate the input of modified water masses from Filchner-Ronne Ice shelf (FRIC) and LCIS
171 (Gordon et al. 1993; Schröder et al. 2002; Schodlok et al. 2002). The hypothesized circulation at LCIS (Nicholls
172 et al. 2004; Hutchinson et al. 2020) is shown by the dashed blue arrow in insert (a). The 3.125 km sea-ice
173 concentration data shown in the central panel were taken from ftp://ftp-projects.cen.uni-
174 hamburg.de/seaice/AMSR2/3.125km and the bathymetry data (inserts a and b) were taken from ETOPO1 (NOAA
175 National Geophysical Data Center 2009).
176

177 Seawater was collected from discrete depths using a rosette of twenty-four 12 L Niskin bottles. At each CTD
178 station, seawater samples for nutrient analysis were collected throughout the water column (typically at 15 discrete
179 depths), while samples for phytoplankton taxonomy and rate experiments were taken from 3-6 depths (see below)
180 that were selected based on profiles of temperature, fluorescence and PAR measured during the CTD down-casts.
181

182 Simulated *in situ* experiments were conducted to determine the rates of net primary production (NPP), N uptake
183 (as nitrate (NO_3^-), ammonium (NH_4^+), and urea-N), and nitrite (NO_2^-) oxidation (a measure of nitrification). For
184 NPP and N uptake, seawater was collected from three depths coinciding with the 55%, 10% and 1% PAR levels,
185 then pre-screened through a 200 μm mesh to remove large grazers and transferred to six 1 L and six 2 L
186 polycarbonate bottles per depth. ^{15}N-labeled NO_3^-, NH_4^+, or urea-N was added to four of the twelve bottles (i.e.,
187 two 1 L and two 2 L bottles per N species) and $NaH^{13}CO_3$ was added to the bottles amended with ^{15}N-NH_4^+. The
188 tracers were added at ~5-10% of the assumed ambient concentrations, yielding final concentrations in each bottle
189 of approximately 100 μM $NaH^{13}CO_3$, 1 μM ^{15}N-NO_3^-, 0.05 μM ^{15}N-NH_4^+, and 0.1 μM ^{15}N-urea-N. Bottles were

https://doi.org/10.5194/bg-2021-122
Preprint. Discussion started: 17 May 2021
© Author(s) 2021. CC BY 4.0 License.

incubated on the deck for 4-6 hours in a custom-built incubator that was cooled with running surface (~7 m) seawater and equipped with neutral density filters to simulate the relevant light levels. Experiments were terminated via filtration onto 0.3 µm combusted (450°C for 8 hours) glass fibre filters (Sterlitech GF-75) that were stored frozen in combusted (500°C for 5 hours) foil envelopes at -80˚C pending analysis.

Seawater samples for the NO_2^- oxidation experiments were collected from the 55%, 10% and 1% light levels, just below the MLD, and at 200 m and 500 m. From each depth, seawater was transferred into duplicate 250 mL opaque high-density polyethylene (HDPE) bottles to which $^{15}N\text{-}NO_2^-$ was added to achieve a final tracer concentration of 0.1 µM. An initial 50 mL subsample ($T_{initial}$) was collected from each HDPE bottle immediately following tracer addition and frozen at -20°C until analysis ashore. The 55%, 10%, 1% and MLD sample bottles were incubated in the on-deck incubator for 20-30 hours while the 200 m and 500 m samples were incubated in a ~2°C cold room. The experiments were terminated by collection and freezing of 50 mL T_{final} subsamples.

2.2. Nutrients

2.2.1. Nutrient concentration analysis

$NO_3^-+NO_2^-$ and silicic acid ($Si(OH)_4$) concentrations were measured using a Lachat QuickChem flow injection analysis platform following published auto-analysis protocols (Diamond 1994; Grasshoff 1976) in a configuration with a detection limit of 0.5 µM. Duplicate samples were measured for $NO_3^-+NO_2^-$ and $Si(OH)_4$ on different days, and the standard deviation for duplicates was ≤0.5 µM, with a lower standard deviation for lower-concentration samples. NO_3^- concentrations were determined by subtraction of NO_2^- from $NO_3^-+NO_2^-$. Concentrations of phosphate (PO_4^{3-}) and NO_2^- were measured shipboard by standard benchtop colourimetric methods (Strickland and Parsons 1968; Bendschneider et al. 2020; Parsons et al. 1984) using a Thermo Scientific Genesis 30 Visible spectrophotometer. The detection limit was 0.05 µM and the standard deviation for duplicate samples was ≤0.05 µM. Aliquots of a certified reference material (JAMSTEC; Lot CG) were analysed during autoanalyser and manual runs to ensure measurement accuracy.

NH_4^+ concentrations were measured ~~ship~~board following the fluorometric method of Holmes et al. (1999) using a Turner Designs Trilogy fluorometer equipped with a UV module. The detection limit was <0.05 µM and the standard deviation for duplicate samples was ≤0.05 µM. The matrix effect (ME) that results from the calibration of seawater samples with Milli-Q water standards was calculated using the standard addition method (Saxberg and Kowalski 1979). All samples were corrected for the ME (Taylor et al. 2007), which was always <10% and typically ≤5%. Urea-N concentrations were measured following the colourimetric method of Revilla et al. (2005) using a Thermo Scientific Genesis 30 Visible spectrophotometer equipped with either a 1 cm- or 5 cm-pathlength cell. The detection limit was 0.05 µM and the standard deviation for duplicate samples was ≤0.05 µM. Hereafter, we use "urea" when referring to urea-N.

2.2.2. Estimating nutrient depletion

The net decrease in euphotic zone nutrient concentrations following nutrient recharge in winter (i.e., the extent of nutrient depletion due to consumption by phytoplankton), between the start of the growing season until the time of our sampling, can be estimated for each station as:

https://doi.org/10.5194/bg-2021-122
Preprint. Discussion started: 17 May 2021
© Author(s) 2021. CC BY 4.0 License.

$$\text{X depletion} = [X]_{measured} - [X]_{source} \quad (1)$$

where $[X]_{source}$ is the average $[NO_3^-]$, $[Si(OH)_4]$ or $[PO_4^{3-}]$ in winter water (WW; a shallow temperature minimum layer underlying ASW that is the remnant of the winter surface mixed layer and considered representative of the pre-bloom surface conditions) and $[X]_{measured}$ is the measured nutrient concentration (Le Corre and Minas 1983; Jennings et al. 1984; Goeyens et al. 1995; Rubin et al. 1998; Hoppema et al. 2007).

Seasonal melting of sea-ice in the Weddell Sea introduces low-salinity, low-nutrient waters to the mixed layer (Eicken 1993), potentially leading to an overestimate of phytoplankton-driven nutrient depletion. We thus correct X depletion for the effect of ice melt as:

$$\text{X depletion}_{(corrected)} = \text{X depletion} - \text{X depletion}_{(melt\ water)} \quad (2a)$$

where $\text{X depletion}_{(melt\ water)}$ is the decrease in the surface $[NO_3^-]$, $[Si(OH)_4]$ or $[PO_4^{3-}]$ due to sea-ice melt (i.e., the dilution effect), calculated as:

$$\text{X depletion}_{(melt\ water)} = [X]_{source} - [X]_{melt\ water} \quad (2b)$$

where:

$$[X]_{melt\ water} = [X]_{sea\text{-}ice}\,(f_{sea\text{-}ice}) + [X]_{source}(1\text{-}f_{sea\text{-}ice}) \quad (2c)$$

Here, the nutrient concentrations in summertime sea-ice ($[X]_{sea\text{-}ice}$) are assumed to be: $[NO_3^-]_{sea\text{-}ice}$ = 1 µM, $[Si(OH)_4]_{sea\text{-}ice}$ = 5 µM, and $[PO_4^{3-}]_{sea\text{-}ice}$ = 0.3 µM (Fripiat et al. 2014), and:

$$f_{sea-ice} = \frac{\text{salinity}_{measured} - \text{salinity}_{source}}{\text{salinity}_{measured} - \text{salinity}_{sea-ice}} \quad (2d)$$

with $\text{salinity}_{sea\text{-}ice}$ taken to be 5 based on measurements made during the cruise and salinity_{source} set to 34.2 at FIS and 34.4 at the other stations (the salinity of WW; Figure 2c insert). On average, correcting for sea-ice melt changed the estimates of X depletion by 0.4 ± 0.9%.

The approach outlined above for calculating $\text{X depletion}_{(corrected)}$ assumes, following correction for sea-ice melt, that nutrient drawdown is due to phytoplankton assimilation only, a reasonable assumption in the Weddell Sea in summer.

2.3. Uptake rates

Incubation filters were oven-dried for 24 hours at 40°C, then folded into tin cups. Samples were analysed using a Flash Elemental Analyser 1112 Series coupled to a Delta V Plus isotope ratio mass spectrometer (IRMS) in a configuration with a detection limit of 2 µg C and 1 µg N. Blanks (combusted unused filters + tin cups) and laboratory running standards, calibrated to certified IAEA reference materials, were run after every five samples.

https://doi.org/10.5194/bg-2021-122
Preprint. Discussion started: 17 May 2021
© Author(s) 2021. CC BY 4.0 License.

The specific rates of carbon fixation (V_C) and NO_3^-, NH_4^+ and urea uptake ($V_{NO_3^-}$, $V_{NH_4^+}$, V_{urea}; d^{-1}) were calculated according to equation 2 in Dugdale and Wilkerson (1986). NPP and the absolute rates of NO_3^-, NH_4^+ and urea uptake (ρNO_3^-, ρNH_4^+ and ρurea; μM d^{-1}) were then determined by multiplying V_C by the concentration of particulate organic carbon ([POC]) and $V_{NO_3^-}$, $V_{NH_4^+}$ and V_{urea} by the concentration of particulate organic nitrogen ([PON]) (Dugdale and Wilkerson 1986; equation 3).

2.4. NO_2^- oxidation rates

The $T_{initial}$ and T_{final} samples collected from the NO_2^- oxidation incubations were measured for the $\delta^{15}N$ of NO_3^- ($\delta^{15}N_{NO3}$; where $\delta^{15}N = (({}^{15}N_{sample}/{}^{14}N_{sample})/({}^{15}N_{standard}/{}^{14}N_{standard}) - 1) \times 1000$) using the denitrifier method (Sigman et al. 2001; McIlvin and Casciotti 2011). Prior to isotopic analysis, all samples were treated with sulfamic acid to remove NO_2^- as the denitrifier method converts both NO_2^- and NO_3^- to N_2O gas (Granger and Sigman 2009); the difference in $\delta^{15}N_{NO3}$ between the T_{final} and $T_{initial}$ samples was then taken as the $^{15}NO_3^-$ enrichment due to $^{15}NO_2^-$ oxidation (Peng et al. 2015). Results were referenced to atmospheric N_2 using certified reference materials (IAEA-NO-3, USGS-34, and USGS-32; Gonfiantini 1984; Böhlke and Coplen 1995; Böhlke et al. 2003). The rate of NO_2^- oxidation ($V_{NO_2^-}$; nM d^{-1}) was calculated following Peng et al. (2015) as:

$$V_{NO_2^-} = \frac{\Delta[{}^{15}NO_3^-]}{f_{NO_2^-}^{15} \times t} \quad (3)$$

where $\Delta[{}^{15}NO_3^-]$ is the difference in the concentration of $^{15}NO_3^-$ between the end and the start of the experiment (i.e., $T_{final} - T_{initial}$) due to NO_2^- oxidation, $f_{NO_2^-}^{15}$ is the fraction of $^{15}NO_2^-$ at the start of the incubation, and t is the length of the incubation (days). The detection limit for $V_{NO_2^-}$ ranged from 0.06-0.46 nM d^{-1} (calculated following Santoro et al. 2013). We take $V_{NO_2^-}$ as an appropriate measure of the nitrification rate given that NO_2^- oxidation is the step in the nitrification pathway that produces NO_3^-.

To determine relative carbon export potential at each station, we calculated the f-ratio (a measure of new production relative to total (i.e., new+regenerated) production) using the absolute N uptake and NO_2^- oxidation rates and a modified version of the Eppley and Peterson (1979) equation:

$$\text{f-ratio}_{(\text{excluding urea})} = \frac{\rho NO_3^- - V_{NO_2^-}}{\rho NO_3^- + \rho NH_4^+} \quad (4a)$$

$$\text{f-ratio}_{(\text{including urea})} = \frac{\rho NO_3^- - V_{NO_2^-}}{\rho NO_3^- + \rho NH_4^+ + \rho urea} \quad (4b)$$

Equation 4 accounts for euphotic zone nitrification ($V_{NO_2^-}$), which yields regenerated rather than new NO_3^- that is then available for phytoplankton to consume. Not accounting for $V_{NO_2^-}$ could result in the f-ratio being overestimated. Equation 4b accounts for urea uptake, that was either measured (at the LCIS stations and WG1) or calculated (at the AP, FIS and WG2) using equation 7 (see section 3.3.4 below).

https://doi.org/10.5194/bg-2021-122
Preprint. Discussion started: 17 May 2021
© Author(s) 2021. CC BY 4.0 License.

307 **2.5. Phytoplankton taxonomy and carbon biomass**

308 At all stations, microphytoplankton samples were collected between the surface and 30 m using a HYDROBIOS
309 conical plankton net (r = 12.5 cm; h = 50 cm) with a mesh size of 55 µm. Samples were transferred to 50 mL
310 centrifuge tubes, fixed with 10 µL of 25% glutaraldehyde and stored at room temperature in the dark until later
311 analysis via light and scanning electron microscopy. Additionally, samples for flow cytometry were collected in
312 50 mL centrifuge tubes from Niskin bottles fired at the 55%, 10% and 1% light depths. These samples were fixed
313 with 10 µL of 25% glutaraldehyde and stored at 4°C until analysis.
314
315 In the onshore laboratory, each preserved net-sample was homogenized, and one drop (40 µL) was wet mounted
316 on a slide. All the cells on the slide with intact chloroplasts (i.e., alive at the time of sampling) were counted at
317 400x or 630x magnification using a Zeiss AxioScope A1 light microscope (LM). The number of cells/L was
318 calculated as:
319
320 $$\text{cells per litre} = A\left(\frac{1}{L}\right)\left(\frac{n}{V}\right) \quad (5)$$
321
322 where A = number of cells per drop; L = volume of water sampled (1470 L; computed using the volume of a
323 cylinder, $\pi\, r^2 h$, where r = 0.125 m and h = 30 m depth); n = volume of the concentrated sample; and V = volume
324 of 1 drop.
325
326 An aliquot of 5 mL from each preserved sample was cleaned by removing carbonate particles and organic matter
327 using 10% hydrochloric acid and 37% hydrogen peroxide, respectively. After thorough rinsing with distilled
328 water, permanent slides were prepared by pipetting the cleaned material onto acid-washed coverslips, air drying
329 overnight and mounting the cover slips onto glass slides using Naphrax® mountant (refractive index = 1.7). The
330 permanent slides were examined using a Zeiss AxioScope A1 LM equipped with differential interference contrast
331 (DIC) at 1000x magnification (under oil immersion) for identification of the diatom cells to the lowest taxonomic
332 classification possible. Stubs were also prepared from the cleaned material for Scanning Electron Microscopy
333 (SEM), with a JEOL JSM 7001F field emission SEM used to visualize the morphological features not evident
334 under LM.
335
336 The average size (µm) and carbon content (pg C $cell^{-1}$) of each identified diatom species was taken from Leblanc
337 et al. (2012) for high latitude locations (50 – 70°S) (Table S1), and the carbon content of colonial *P. antarctica* was
338 estimated as 13.6 pg C $cell^{-1}$ (Mathot et al. 2000) for single cells within a colony. Since the majority of *P.*
339 *antarctica* were in spherical colony form, the total colony carbon biomass (C_{COL}) was calculated as:
340
341 $$C_{COL} = [13.60 \times N_C] + C_M \quad (6)$$
342
343 where N_C is the number of cells counted per litre; C_M is the mucus-related carbon calculated as $C_M = 0.213 \times V_{COL} + 4.58$; and V_{COL} is the volume of the spherical colony, calculated as $V_{COL} = 417 \times N_C^{1.67}$ (Mathot et al.
344
345 2000).
346

https://doi.org/10.5194/bg-2021-122
Preprint. Discussion started: 17 May 2021
© Author(s) 2021. CC BY 4.0 License.

All flow cytometry samples were analyzed using a BD LSR II SORP flow cytometer with blue/red/green laser configuration. Prior to analysis, sample tubes were gently agitated to homogenize the contents, then 1 mL of sample was transferred to a 5 mL polycarbonate test tube. The size-class to which each cell belonged was defined based on its forward scatter area (FSC-A) relative to the FSC-A of 2.8 µm and 20 µm beads (Figure S1a). Once categorized as either picoplankton (<2.8 µm), nanoplankton (2.8-20 µm) or microplankton (>20 µm), the cells were grouped into six populations based on their orange fluorescence (indicative of phycoerythrin; PE) relative to their red fluorescence (indicative of chlorophyll-a; chl-a): two *Synechococcus* populations (Syn 1 and Syn 2), one picoeukaryote population (PicoEuk), two nanoeukaryote populations (NanoEuk 1 and NanoEuk 2), and one microeukaryote population (MicroEuk; see section S2 in the Supplemental Information for details of population identification). The biovolumes of the eukaryotic populations were estimated based on their FSC-A relative to that of six beads of known size and volume (Figure S1c; Table S2). *Synechococcus* had an unrealistically high FSC-A, which is an artefact of this group having a high ratio of photosystem I to photosystem II compared to the other phytoplankton populations. This increases electron chain activity, leading to an increase in the emission spectrum and low excitation of the *Synechococcus* populations (Kaprelyants and Kell 1993; Sunda and Huntsman 2015). The biovolume of *Synechococcus* was thus assumed to be 1 μm^3 (Kana and Glibert 1987; Paulsen et al. 2015). Biovolume is taken here as a proxy for biomass.

3. Results

3.1. Water column hydrography

Throughout the study region, relatively cool and fresh (-2 to 0°C and 33.0 to 34.5) ASW occurred between the surface and 135 m (Figure 2). Through this layer and down to 200 m, salinity increased with depth while temperature decreased, reaching a local minimum (-1.6°C) at ~100 m. These hydrographic changes are characteristic of WW, which is considered a summertime record of winter conditions and a reflection of the initial state from which the mixed layer evolves over the spring/summer growing season (Altabet and Francois 2001). Below WW ~~at the AP and WG stations~~, salinity remained constant while temperature increased with depth, reaching a local maximum (0.5°C) at 500 m and 300 m for the AP and WG, respectively. This feature is characteristic of Warm Deep Water (WDW), a temperature maximum layer that is a modified form of Circumpolar Deep Water (CDW) (Muench and Gordon 1995; Fahrbach et al. 1995). Below WW at the LCIS and FIS stations, salinity increased and temperature decreased with depth, reaching a local salinity maximum (34.6 at LCIS and 34.3 at FIS) and temperature minimum (≤ -1.8°C). The increase in salinity is characteristic of High Salinity Shelf Water (HSSW) produced by brine rejection during sea-ice formation, while the decrease in temperature is characteristic of Ice Shelf Water (ISW) produced by the supercooling of ASW under the ice shelves (Fahrbach et al. 1995; Nicholls et al. 2009; Hutchinson et al. 2020). The densities of WW,WDW, HSSW and ISW are contiguous, with the mixed product of these waters termed Modified Warm Deep Water (MWDW) (Fahrbach et al. 1995). Below WDW at the AP and WG stations, temperature decreased due to the presence of Weddell Sea Deep Water (WSDW; temperature range of -0.7 to 0°C) and Weddell Sea Bottom Water (WSBW; temperature ≤ -0.7°C) (Fahrbach et al. 1995; Muench and Gordon 1995).

Variability in the density of ASW was observed among the stations (Figure 2a). The surface density profiles at the AP, WG and early-summer FIS stations were very similar, while the late-summer density profile at FIS

https://doi.org/10.5194/bg-2021-122
Preprint. Discussion started: 17 May 2021
© Author(s) 2021. CC BY 4.0 License.

revealed lower-density waters ~~over~~ the upper 100 m. At LCIS, the surface density profiles were highly variable, and no consistent pattern was observed, although the most northern stations (L9 and L10; Figure 1) were characterised by the lowest densities. Stations L1 and L3, situated closest to the ice shelf, were characterised by the highest densities, contiguous with the underlying WW layer.

The MLD appeared most strongly controlled by salinity at all stations and was always shallower than the depth of the euphotic zone (Z_{eu}; Table 1), the latter defined as the depth ~~to which~~ 1% of surface PAR ~~penetrated~~ (Kirk 1994). The deepest MLD and Z_{eu} were observed at FIS in early summer (average MLD of 103 ± 36.6 m and Z_{eu} of 91.7 ± 14.4 m; n = 3), while the shallowest MLD and Z_{eu} were observed at LCIS (average MLD of 13.9 ± 5.9 m and Z_{eu} of 28.5 ± 9.1 m; n = 10) (Figure 2d; Table 1). The rates of NPP, N uptake and nitrification were ~~therefore~~ trapezoidally-integrated to Z_{eu} rather than to the MLD since we assume that phytoplankton were active at least to the depth of 1% PAR.

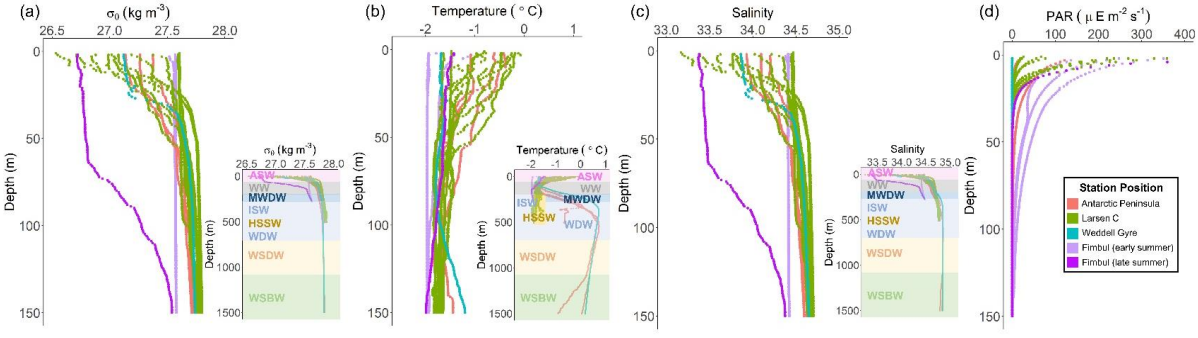

Figure 2. Depth profiles (0-100 m) of (a) potential density (σ_0), (b) potential temperature, (c) absolute salinity, and (d) photosynthetically active radiation (PAR) at all stations. The inserts in panels (a), (b) and (c) show the profiles down to 1500 m, with the various water masses present at each station identified from their temperature and salinity ranges (WSBW – Weddell Sea Bottom Water, WSDW – Weddell Sea Deep Water, WDW – Warm Deep Water, MWDW – Modified Warm Deep Water, ISW – Ice Shelf Water, HSSW – High Salinity Shelf Water, WW – Winter Water, ASW – Antarctic Surface Water). The station positions are indicated by the different colours: red – Antarctic Peninsula, green – Larsen C Ice Shelf, blue –Weddell Gyre, light purple – early summer Fimbul Ice Shelf, and dark purple – late summer Fimbul Ice Shelf.

3.2. Nutrient concentrations

The concentrations of the regenerated N forms (i.e., NH_4^+ and urea) were generally low in the surface and increased with depth to reach a maximum below Z_{eu}, before decreasing again to below detection by 200-300 m (Figure 3a and b; Table 1). A sharp maximum in the NH_4^+ concentration was observed at Z_{eu} at all stations, indicative of the depth of maximum net remineralisation. Urea was more variable, likely due to variability in the processes that produce this N form (e.g., bacterial excretion; Berges and Mulholland 2008). The highest average concentrations of regenerated N in the euphotic zone were observed at LCIS and FIS in late summer (0.62 ± 0.30 µM for NH_4^+ and 0.21 ± 0.07 µM for urea), while the lowest concentrations were observed at FIS in early summer (below detection for both NH_4^+ and urea). Elevated regenerated N concentrations were also observed at the AP stations (euphotic zone average of 0.8 ± 0.3 µM for NH_4^+ and 0.2 ± 0.06 µM for urea), while low concentrations were observed at the WG stations (euphotic zone average of 0.3 ± 0.1 µM for NH_4^+ and 0.1 ± 0.0 µM for urea).

https://doi.org/10.5194/bg-2021-122
Preprint. Discussion started: 17 May 2021
© Author(s) 2021. CC BY 4.0 License.

The concentrations of NO_2^- were generally low throughout the euphotic zone, and decreased to below detection ~~by~~ 120 m at the FIS, AP, and WG stations (with the exception of a single sample from the early-summer FIS), and ~~by~~ 500 m at LCIS (Figure 3c). A high degree of variability was observed, ~~with the highest~~ surface-layer NO_2^- concentrations occurring in the WG and at FIS in late summer (average euphotic zone NO_2^- concentrations of 0.08 ± 0.06 µM and 0.12 ± 0.03 µM, respectively).

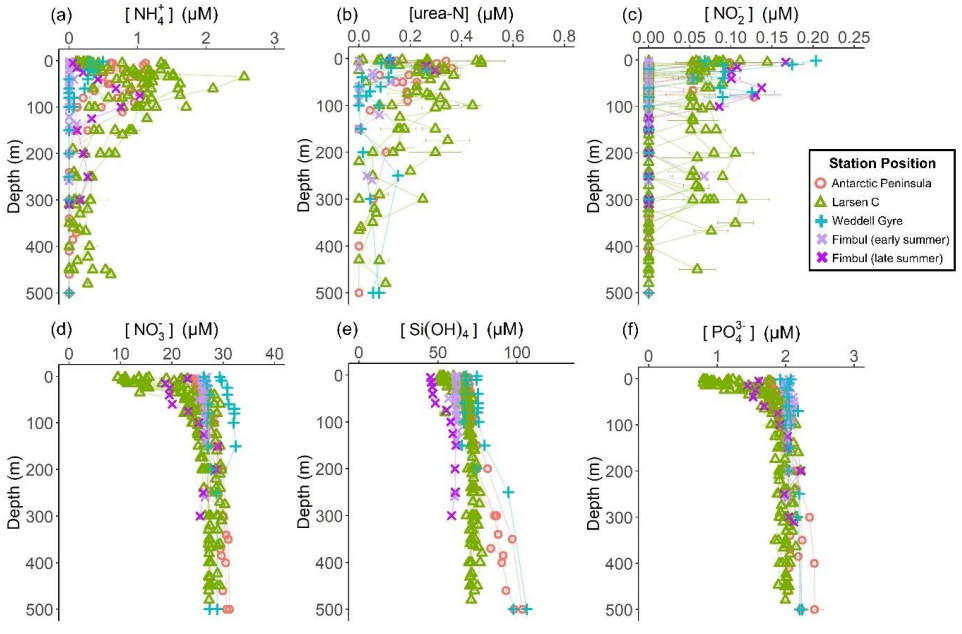

Figure 3. Depth profiles (0-500 m) of ~~the concentrations of~~ (a) NH_4^+, (b) urea-N, (c) NO_2^-, (d) NO_3^-, (e) $Si(OH)_4$ and (f) PO_4^{3-}. For all panels, the error bars represent ± 1 SD replicate samples (n = 2-3). Where applicable, the error has been propagated according to standard statistical practices.

The euphotic zone concentrations of NO_3^-, $Si(OH)_4$ and PO_4^{3-} decreased towards the surface due to assimilation by phytoplankton (Figure 3d-f). The lowest surface concentrations of NO_3^- and PO_4^{3-} were observed at LCIS (16.6 ± 3.8 µM and 1.3 ± 0.4 µM, respectively) and of $Si(OH)_4$ ~~was observed~~ at FIS in late summer (46.1 ± 0.8 µM). The highest surface concentrations of NO_3^-, PO_4^{3-} and $Si(OH)_4$ occurred in early summer at FIS (26.5 ± 0.32 µM, 2.0 ± 0.04 µM and 61.6 ± 0.5 µM, respectively). ~~Elevated~~ $Si(OH)_4$ and PO_4^{3-} concentrations were observed between 200 and 500 m at the AP and WG stations due to the presence of WDW at these stations versus shelf waters (i.e., ISW and HSSW) at LCIS and FIS. ~~WDW has the longest residence time of all water masses in the Weddell Sea, and has therefore undergone the greatest modification by physical and biogeochemical processes (Whitworth and Nowlin 1987; Hoppema et al. 2015).~~ The depth of maximum remineralisation in the open Weddell Sea is 300-500 m, the depth range occupied by WDW (Vernet et al. 2019, and references therein). The high rates of remineralisation, and therefore nutrient accumulation, in WDW account for the elevated nutrient concentrations observed in WDW relative to the shelf water masses (Whitworth and Nowlin 1987). Estimates of NO_3^-, $Si(OH)_4$ and PO_4^{3-} depletion (i.e., X depletion$_{(corrected)}$; equation 2) were highest at LCIS (average NO_3^- depletion of 8.3 ±

https://doi.org/10.5194/bg-2021-122
Preprint. Discussion started: 17 May 2021
© Author(s) 2021. CC BY 4.0 License.

3.9 µM, $Si(OH)_4$ depletion of 8.3 ± 4.0 µM and PO_4^{3-} depletion of 0.6 ± 0.3 µM), while the lowest nutrient depletions occurred in early summer at FIS (average NO_3^- depletion of 0.3 ± 0.3 µM, $Si(OH)_4$ depletion of 0.6 ± 0.6 µM and PO_4^{3-} depletion of 0.00 ± 0.02 µM) (Figure 4a-c; Table 1).

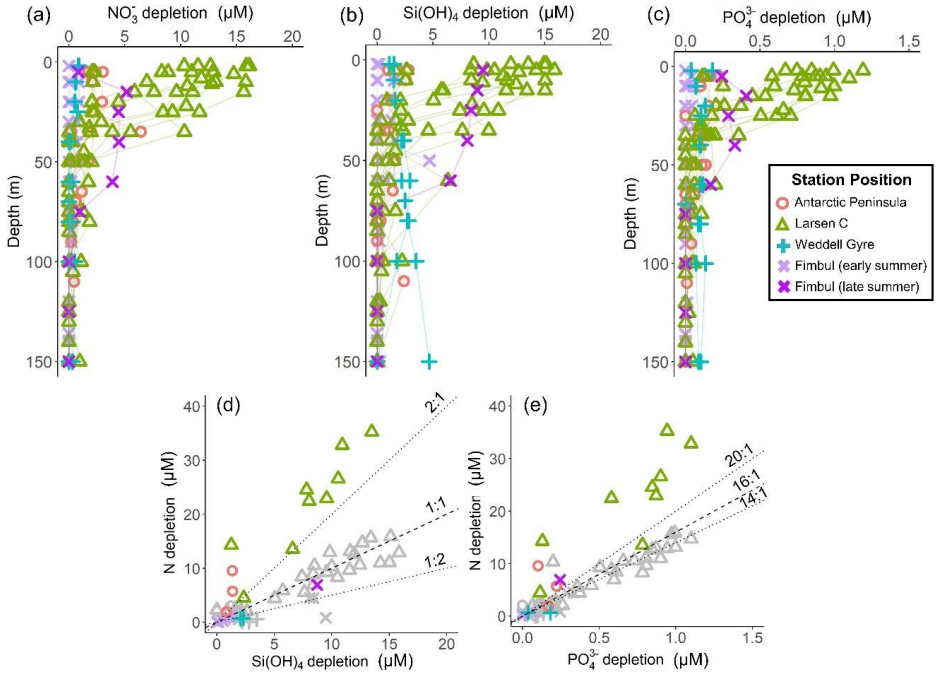

Figure 4. Depth profiles (0-150 m) of (a) NO_3^- ~~depletion~~, (b) $Si(OH)_4$ ~~depletion~~ and (c) PO_4^{3-} depletion at each station. Also shown are scatterplots of (d) $Si(OH)_4$ ~~depletion~~ versus NO_3^- depletion at each depth ~~over~~ the euphotic zone at all stations (grey symbols) and the theoretical euphotic zone-averaged $Si(OH)_4$ versus total N depletion (coloured symbols; see text for details) and (e) PO_4^{3-} ~~depletion~~ versus NO_3^- depletion ~~at each depth over~~ the euphotic zone at all stations (grey symbols) and the theoretical euphotic zone-averaged PO_4^{3-} versus total N depletion (coloured symbols). The dashed line in panel (d) represents the 1:1 Si:N depletion ratio, expected for iron-replete diatoms (Ragueneau et al. 2000; Hutchins and Bruland 1998; Takeda 1998; Mosseri et al. 2008), while the dotted lines represent the 1:2 Si:N ratio, indicative of enhanced activity of non-siliceous phytoplankton, and the 2:1 Si:N ratio, expected for iron-limited diatoms (Arrigo et al. 1999; Franck et al. 2000; Brzezinski et al. 2003; Green and Sambrotto 2006; Mosseri et al. 2008; Weber and Deutsch 2010; Martiny et al. 2013). The dashed line in panel (e) represents the 16:1 N:P depletion ratio (the Redfield ratio), while the dotted lines represent the 20:1 N:P ratio, expected for *P. antarctica*, and 14:1 N:P ratio, expected for iron-replete diatoms (Hutchins and Bruland 1998; Takeda 1998; Arrigo et al. 1999; Ragueneau et al. 2000; Mosseri et al. 2008).

Variations in the depletion ratios of $Si(OH)_4$:NO_3^- and NO_3^-:PO_4^{3-} can be used as indicators of the nutrient status of the phytoplankton community, particularly diatoms. Under iron-replete conditions, diatoms have been observed to consume $Si(OH)_4$ and NO_3^- in a ratio of ~1:1, and NO_3^- and PO_4^{3-} in a ratio of ~14:1 (Hutchins and Bruland 1998; Takeda 1998; Ragueneau et al. 2000; Mosseri et al. 2008), while under conditions of limitation, the ratio of $Si(OH)_4$:NO_3^- uptake rises (to >>2:1) and NO_3^-:PO_4^{3-} uptake decreases (to as low as 10:1) (Arrigo et al. 1999; Franck et al. 2000; Brzezinski et al. 2003; Green and Sambrotto 2006; Mosseri et al. 2008; Weber and Deutsch 2010; Martiny et al. 2013). Additionally, ~~the dominance of one phytoplankton species over another~~ may ~~cause~~

https://doi.org/10.5194/bg-2021-122
Preprint. Discussion started: 17 May 2021
© Author(s) 2021. CC BY 4.0 License.

Biogeosciences Discussions

deviations in the NO_3^-:PO_4^{3-} depletion ratio. For example, in regions dominated by *P. antarctica*, Arrigo et al. (1999) observed a NO_3^-:PO_4^{3-} depletion ratio of ~20:1, while in ~~those~~ dominated by ~~iron-deplete~~ diatoms, ~~it was~~ ~~≈~~10:1. The NO_3^-:PO_4^{3-} depletion ratios can thus also yield ~~insights into the dominant~~ phytoplankton ~~species active in the upper water column~~. In our study, the average euphotic zone $Si(OH)_4$:NO_3^- depletion ratios ranged from 0.5 to 6.1 (Table 1), with the highest ratios estimated for the WG stations (average of 5.4 ± 5.5) and FIS stations F3 and F4 (average of 2.7 ± 2.8; the same station occupied in early- (F3) and late summer (F4)). The euphotic zone average NO_3^-:PO_4^{3-} depletion ratios were more variable, ranging from 3.7 ± 1.5 to 48.6 ± 11.5, with the lowest ratios computed for the WG stations (average of 4.1 ± 1.5) and the highest for FIS in early summer (average of 33.7 ± 3.6).

3.3. Upper ocean biomass, NPP and N uptake rates

3.3.1. Particulate organic carbon and nitrogen

The highest concentrations of POC and PON were observed in the surface at all stations (Figure 5a), decreasing towards Z_{eu} (Figure 5e). Averaged over the euphotic zone, the lowest POC and PON concentrations occurred in early summer at FIS (4.6 ± 1.5 µM and 0.3 ± 0.1 µM, respectively) and the highest at LCIS (17.9 ± 7.3 µM and 2.5 ± 0.8 µM, respectively; Table 2). ~~Across the region, the biomass~~ C:N ratio ~~was~~ fairly uniform throughout the euphotic zone, except at stations F1, F2 and ~~the~~ WG ~~stations~~ (Figure 5b, d and f). In general, the FIS and WG stations were characterized by significantly higher C:N ratios than those expected from Redfield stoichiometry (C:N = 6.63:1), averaging 16.5 ± 8.8 and 12.3 ± 1.8, respectively. At the LCIS stations, ~~the biomass~~ C:N ratios were close to ~~the~~ Redfield r~~atio~~ (7.4 ± 1.9), while the AP stations were characterized by slightly higher C:N ratios (8.3 ± 2.5).

https://doi.org/10.5194/bg-2021-122
Preprint. Discussion started: 17 May 2021
© Author(s) 2021. CC BY 4.0 License.

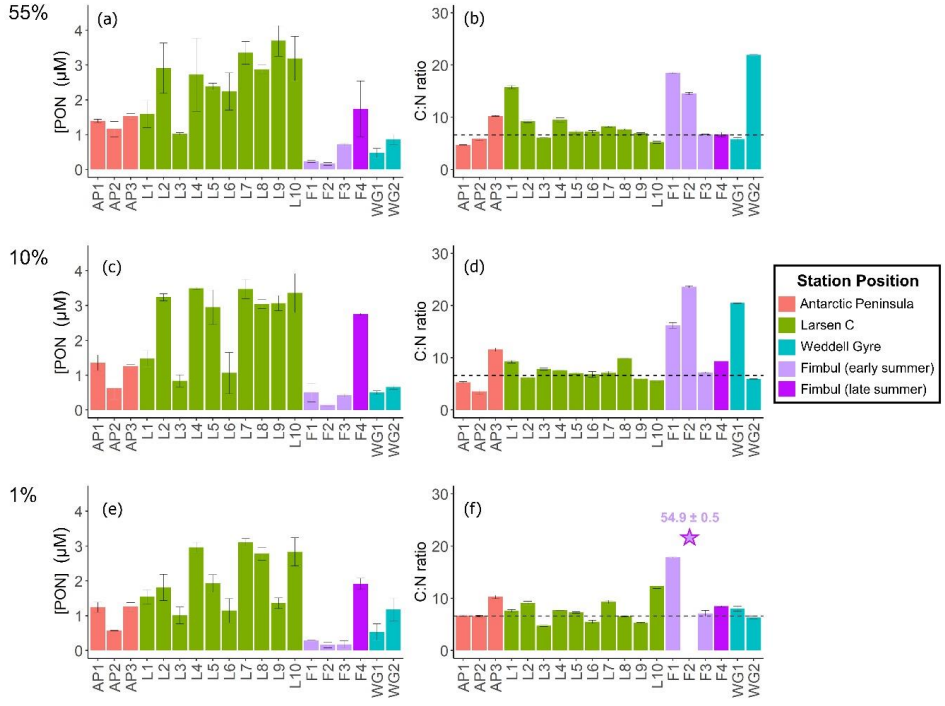

Figure 5. Bar plots of (a, c, e) PON concentrations and (b, d,f) ~~biomass~~ C:N ratios measured at the 55% (a-b), 10% (c-d) and 1% light levels (e-f). The dotted black line in panels (b), (d), and (f) indicates the Redfield C:N ratio of 6.63. The error bars represent ± 1 SD of replicate samples (n = 2-6). Where applicable, the error has been propagated according to standard statistical practices.

3.3.2. ~~Rates of~~ NPP and N uptake

At all stations, NPP was highest at the surface (Figure 6a) and decreased towards Z_{eu} (Figure 6i). The highest depth-specific rates were observed at LCIS (except at station L10 where the rates were very low), while the lowest rates occurred in early summer at FIS (with particularly low rates at station F1; Figure 6a, e and i). At the WG stations and at FIS in late summer, rates of NPP were comparable to the lower end of the rates observed at LCIS, while NPP along the AP increased shoreward to values similar to those at LCIS (i.e., the lowest rates were observed at AP1 and the highest at AP3). The highest euphotic zone-integrated rates of NPP were observed at AP3 (65.0 ± 0.1 mmol m^{-2} d^{-1}) and L5 (61.0 ± 0.7 mmol m^{-2} d^{-1}), while the lowest occurred at L10 (1.8 ± 0.04 mmol m^{-2} d^{-1}) (Table 2).

~~As per~~ NPP, ~~the rates of~~ ρNO_3^- ~~decreased towards~~ Z_{eu} at all stations (Figure 6b, f and j), as did ~~the extent of~~ NO_3^- depletion (Figure 4a). The depth-specific rates of ρNO_3^- were highest at LCIS and lowest in early summer at FIS. However, because the euphotic zone was generally shallower at LCIS than at the other stations, the euphotic zone-integrated rates of ρNO_3^- were fairly similar across the study region, with the largest variability observed at LCIS (Table 2). In late summer at FIS, the rates of ρNO_3^- were on average higher than at LCIS (3.9 ± 0.03 mmol m^{-2} d^{-1} at F4 versus an average of 2.2 ± 1.1 mmol m^{-2} d^{-1} at LCIS), with depth-specific rates that were double those

https://doi.org/10.5194/bg-2021-122
Preprint. Discussion started: 17 May 2021
© Author(s) 2021. CC BY 4.0 License.

513 measured at FIS in early summer. The sea-ice at FIS had completely melted by late summer, which likely
514 contributed to the increase in ρNO_3^- later in the season. The highest euphotic zone-integrated ~~rates of~~ ρNO_3^- were
515 observed at stations F3 and L5 (4.8 ± 0.07 mmol m^{-2} d^{-1} and 4.7 ± 0.04 mmol m^{-2} d^{-1}, respectively). At L5, this
516 elevated rate coincided with low euphotic zone NO_3^- concentrations (12.0 ± 1.9 µM; Figure 3d) and ~~a high degree~~
517 ~~of~~ NO_3^- depletion (10.9 ± 2.3 µM; Figure 4a). The lowest euphotic zone-integrated rates of ρNO_3^- occurred at
518 station L10 (0.5 ± 0.0 mmol m^{-2} d^{-1}).
519
520 Across all stations, rates of ρNH_4^+ increased with depth, reaching a maximum at Z_{eu} (Figure 6c, g and k). The
521 highest ~~depth-specific rates of~~ ρNH_4^+ were observed at LCIS and the lowest at FIS in early summer. Euphotic
522 zone-integrated rates of ρNH_4^+ at the AP stations were comparable to those observed at LCIS (regional average
523 of 3.3 ± 2.2 mmol m^{-2} d^{-1} and 2.5 ± 1.3 mmol m^{-2} d^{-1}, respectively), while the rates at the WG stations and at FIS
524 in late summer were comparable to the lower end of the LCIS rates (~~regional~~ averages of 2.0 ± 0.2 mmol m^{-2} d^{-1}
525 at WG and 1.9 ± 0.0 mmol m^{-2} d^{-1} at FIS). The early- to late-summer rise in the euphotic zone-integrated rates of
526 ρNH_4^+ at FIS coincided with an increase in the average euphotic zone NH_4^+ concentration from below detection
527 to 0.2 ± 0.1 µM (Figure 3a). At the AP, LCIS and WG stations, the rates of ρNH_4^+ were similar to the coincident
528 rates of ρNO_3^-, while at FIS, ρNH_4^+ was less than half ~~of~~ ρNO_3^- (Table 2). The highest euphotic zone-integrated
529 ~~rates of~~ ρNH_4^+ were observed at station AP3 (5.8 ± 0.0 mmol m^{-2} d^{-1}), coincident with high average euphotic zone
530 NH_4^+ (1.1 ± 0 µM). The lowest euphotic zone-integrated rates occurred at station F1 (0.4 ± 0.0 mmol m^{-2} d^{-1})
531 where the concentration of NH_4^+ in the euphotic zone was below detection.
532
533 Rates of ρurea were only measured at the LCIS stations and WG1 (Figure 6d, h and l; Table 2). A high degree of
534 variability in the rates of ρurea was observed at LCIS, with euphotic zone-integrated rates ranging from 0.2 to 1.1
535 mmol m^{-2} d^{-1} (regional average of 0.6 ± 0.3 mmol m^{-2} d^{-1}). This variability appears to be related to the urea
536 concentrations, with the highest rates of ρurea occurring where the ambient urea concentrations were highest (e.g.,
537 station L5), and vice versa (e.g., station L4) (Figure 3b). On average, ~~the rates of~~ ρurea in the WG were half the
538 ~~coincident rates of~~ ρNH_4^+, and urea concentrations were low (Figure 3b; Table 2).

https://doi.org/10.5194/bg-2021-122
Preprint. Discussion started: 17 May 2021
© Author(s) 2021. CC BY 4.0 License.

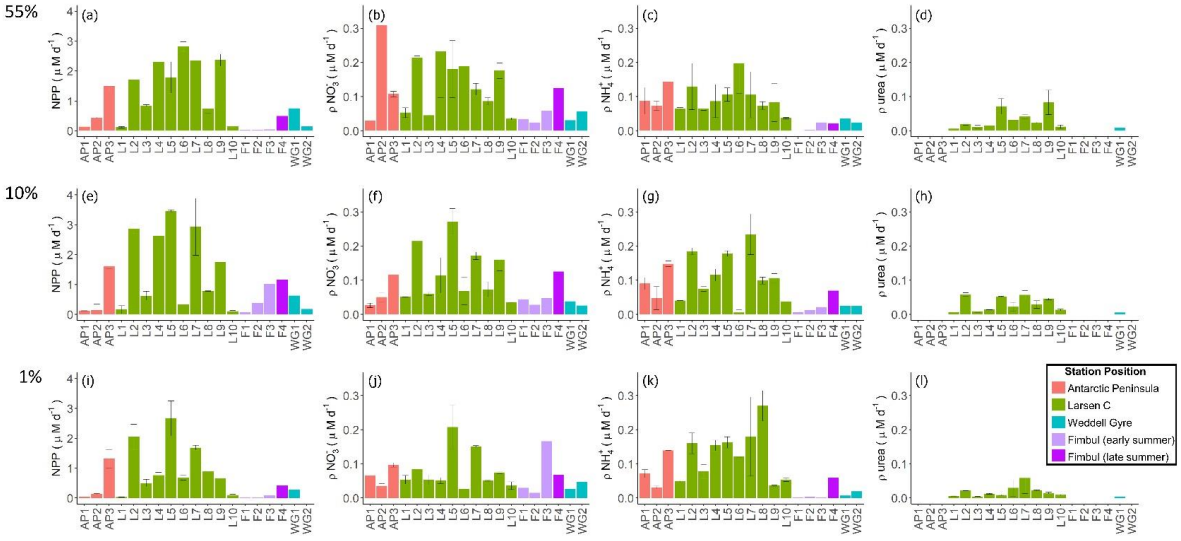

Figure 6. Daily rates of (a, e, i) NPP, (b, f, j) ρNO_3^-, (c, g, k) ρNH_4^+ and (d, h, l) ρurea for the 55% (a-d), 10% (e-h) and 1% light level (i-l). Where there are no bars in panels (d), (h) and (l), no data are available. The error bars represent ± 1 SD of replicate samples (n = 2).

3.3.3. Rates of nitrite oxidation

~~Rates of~~ $V_{NO_2^-}$ were low throughout the euphotic zone across the study region (average of 20.8 ± 31.3 μmol m^{-2} d^{-1}), equivalent to 0 to 3.6% (average of 0.7 ± 1.1%) of ρNO_3^-, and rapidly increased below Z_{eu} (Figure 7). The highest euphotic zone rates were observed at WG1 (average of 6.3 ± 5.0 nM d^{-1}), while the lowest rates occurred at the AP (regional average of 0.0 ± 0.04 nM d^{-1}; Figure 7).

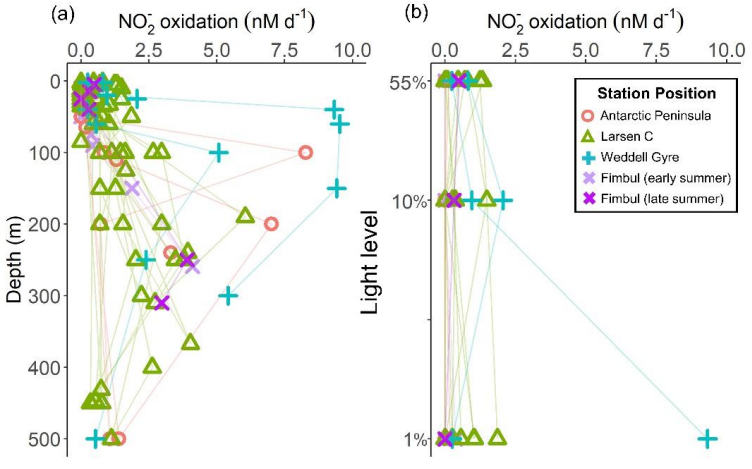

Figure 7. Depth profiles of the NO_2^- oxidation rates measured at each station (a) between the surface and 500 m, and (b) within the euphotic zone only.

https://doi.org/10.5194/bg-2021-122
Preprint. Discussion started: 17 May 2021
© Author(s) 2021. CC BY 4.0 License.

552 **3.3.4. f-ratio estimates**

553 Urea uptake was measured at the LCIS stations and WG1 (at 11 out of 19 stations; Figure 6; Table 2) where it
554 accounted for 8 ± 6% of total N uptake (i.e., ρNO_3^- + ρNH_4^+ + ρurea). Excluding urea uptake when calculating
555 the f-ratio would therefore overestimate the fraction of potentially exportable carbon by ~8%. We estimated urea
556 uptake at the stations where it was not measured as:
557
558 $$\rho urea = (\rho NO_3^- + \rho NH_4^+) \times 0.08 \quad (7)$$
559
560 Equation 7 may overestimate urea uptake at some of the stations, particularly where low urea concentrations were
561 measured. Theoretically, ρurea can also be estimated by assuming that total N uptake should equal NPP/6.63 (i.e.,
562 assuming balanced phytoplankton growth), such that any difference between ρNO_3^- + ρNH_4^+ and NPP/6.63 is due
563 to urea uptake. However, this approach underestimated urea uptake at all the stations where it was directly
564 measured. We therefore chose to use equation 7 to estimate urea uptake for the stations lacking ρurea
565 measurements as this approach will yield a more conservative (i.e., lower) estimate of the fraction of potentially
566 exportable carbon. Figure 8 shows how including urea uptake affected the f-ratio throughout the sample region,
567 with the white (no urea uptake measured) and hashed bars (urea uptake measured) indicating the amount by which
568 the f-ratio decreased when urea uptake was included (i.e., equation 4b versus equation 4a).
569
570 The euphotic zone-integrated f-ratios were highest at FIS in early summer (average $\text{f-ratio}_{(\text{excluding urea})}$ of 0.79 ±
571 0.1 and $\text{f-ratio}_{(\text{including urea})}$ of 0.73 ± 0.09) and lowest at LCIS (average $\text{f-ratio}_{(\text{excluding urea})}$ of 0.50 ± 0.09 and f-
572 $\text{ratio}_{(\text{including urea})}$ of 0.47 ± 0.08) (Figure 8; Table 2). The variability in the f-ratios among stations appears to be
573 related to the availability of NH_4^+. For example, at FIS in early summer there was no NH_4^+ available to the
574 phytoplankton and the highest f-ratios were observed (average $\text{f-ratio}_{(\text{excluding urea})}$ of 0.82 ± 0.08 and $\text{f-ratio}_{(\text{including}}$
575 $_{\text{urea})}$ of 0.76 ± 0.07), while in late summer, NH_4^+ concentrations were elevated (0.2 ± 0.1 µM) and the f-ratio
576 declined ($\text{f-ratio}_{(\text{excluding urea})}$ of 0.68 ± 0.16 and $\text{f-ratio}_{(\text{including urea})}$ of 0.63 ± 0.15).

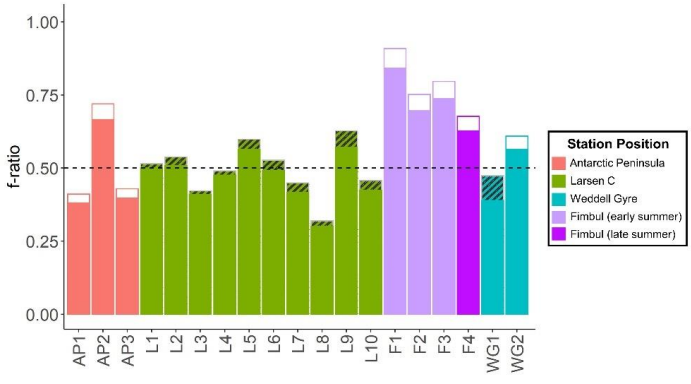

577

578 **Figure 8.** Euphotic zone-integrated f-ratios at each station. The hashed and white bars show the difference
579 between the $\text{f-ratio}_{(\text{excluding urea})}$ (higher value) and the $\text{f-ratio}_{(\text{including urea})}$ (lower value), with the hashed bars
580 representing the stations where urea uptake was measured and the white bars where it was estimated (see text for
581 details).

https://doi.org/10.5194/bg-2021-122
Preprint. Discussion started: 17 May 2021
© Author(s) 2021. CC BY 4.0 License.

582
583 **3.3.5. Phytoplankton community composition**
584 ~~The flow cytometry data suggest that~~ the phytoplankton community was numerically dominated by picoplankton
585 at all stations, with *Synechococcus* emerging as the most abundant group (59 ± 19% of the total phytoplankton
586 cells counted), except at stations L5 and L6 where picoeukaryotes were dominant (51 ± 1%; Figure 9a-b). The
587 microeukaryotes were the least abundant group at all stations (average abundance across the sampling region of
588 8 ± 3%); however, due to their large biovolume, they contributed most to the biomass (average contribution to
589 biomass across the sampling region of 80 ± 7 %; Figure 9c). In the configuration used here, flow cytometry is best
590 suited for enumerating small cells (<15 µm; Dubelaar and Jonker 2000), such that the larger microplankton ~~present~~
591 ~~at the time of sampling~~ were likely underestimated via this technique. ~~We thus take the phytoplankton net~~
592 ~~collections as more representative of the microplankton community and colonial nanoplankton groups~~.
593
594 From the samples collected using the phytoplankton net (i.e., single or colonial cells >55 µm), the dominant
595 phytoplankton species at LCIS was the prymnesiophyte, *P. antarctica* (83 ± 17% of the total phytoplankton cells
596 counted), while the phytoplankton community at the other stations was dominated by diatoms (mainly *Corethron*
597 *pennatum*, *Chaetoceros spp.* (six species), *Cylindrotheca closterium*, *Fragilariopsis ritscheri*, *Fragilariopsis*
598 *curta*, *Fragilariopsis kerguelensis*, *Fragilariopsis rhombica*, *Leptocylindrus mediterraneus*, *Odontella weisflogii*,
599 *Pseudo-nitzschia alanata* and several *Thalassiosira* spp., constituting 92 ± 6% of the total phytoplankton cells
600 counted; Figure 9d-e). At LCIS, the stations sampled earlier in the season tended to be dominated by *P. antarctica*
601 (e.g., station L3) while those sampled later hosted a more diatom-dominated community (e.g., station L8). In
602 addition, the resident diatoms at LCIS (mainly *F. ritscheri*, *O. weisflogii* and *Thalassiosira* spp.) were much larger
603 than the numerically dominant *P. antarctica* (by ~30- to 50-fold). For example, at station L8, the 32 diatom species
604 present (1603 cells L^{-1}) contributed 1.80 pg C L^{-1} (Leblanc et al. 2012) compared to 0.14 pg C L^{-1} resulting from
605 the 7812 cells L^{-1} of *P. antarctica* (Mathot et al. 2000). The LCIS stations with the highest relative abundance of
606 diatoms (e.g., station L8) were characterized by some of the highest rates of ρNO_3^- and greatest extent of NO_3^-
607 depletion. More broadly, the LCIS stations with the lowest SSTs and nutrient uptake rates (i.e., stations L1 and
608 L3) had the lowest phytoplankton counts, while those with the highest SSTs and nutrient uptake rates (i.e., station
609 L5) had the highest phytoplankton counts (Figure 9a and d; Table 1).
610
611

https://doi.org/10.5194/bg-2021-122
Preprint. Discussion started: 17 May 2021
© Author(s) 2021. CC BY 4.0 License.

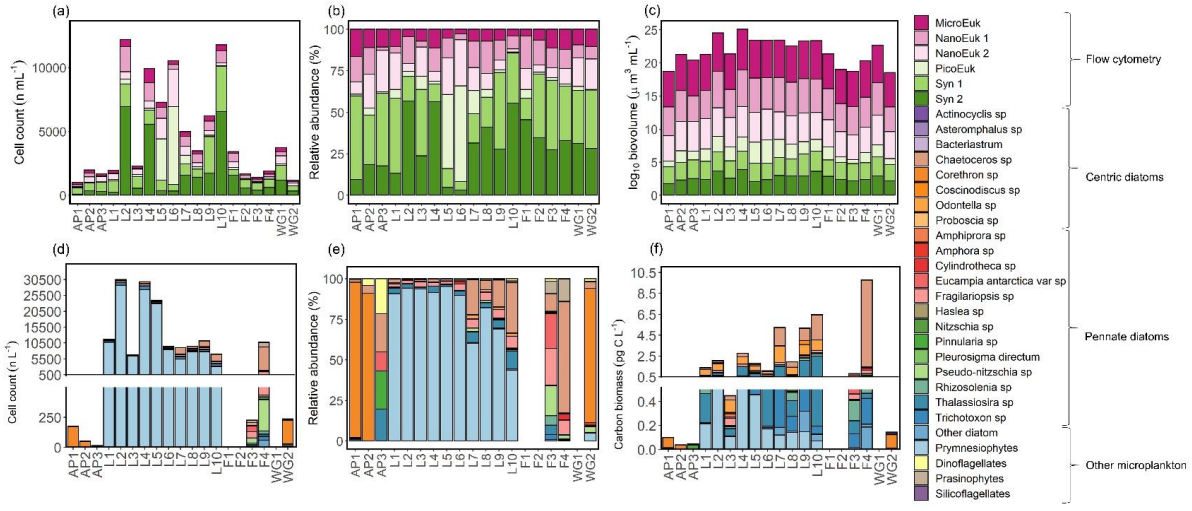

Figure 9. The (a, d) cell counts, (b, e) relative cell abundance**,** (c) log-transformed biovolume and (f) carbon biomass of all phytoplankton groups identified from the (a-c) surface flow cytometry samples and (d-f) phytoplankton net samples. Where there are no bars in panels (d), (e), and (f), no data are available. Carbon biomass estimates in panel (f) are only available for the prymnesiophyte, *P. antarctica*, and the diatom species.

https://doi.org/10.5194/bg-2021-122
Preprint. Discussion started: 17 May 2021
© Author(s) 2021. CC BY 4.0 License.

Biogeosciences
Discussions
Open Access
EGU

616

Table 1. Euphotic zone-averaged nutrient concentrations, nutrient depletions, and nutrient depletion ratios at each station occupied in the Weddell Sea in summer 2018/2019. Values shown are averages ± 1 SD ($n \geq 2$). "-" indicates no available data.

Station position	Station	Sampling date	MLD (m)	Z_{eu} (m)	NH_4^+ (µM)	Urea-N (µM)	NO_3^- (µM)	NO_3^- depletion (µM)	$Si(OH)_4$ depletion (µM)	PO_4^{3-} depletion (µM)	$Si(OH)_4$:NO_3^- depletion	NO_3^-:PO_4^{3-} depletion
FIS Average	**FIS**		**82 ± 51**	**79 ± 28**	**0.1 ± 0.1**	**0.1 ± 0.1**	**25.0 ± 2.8**	**0.7 ± 1.4**	**1.6 ± 3.0**	**0.1 ± 0.1**	**2.0 ± 1.1**	**26.4 ± 19.8**
Fimbul	F1	01/01/19	135	100	0.0 ± 0.0	-	26.4 ± 0.5	0.2 ± 0.5	0.5 ± 1.6	0.0 ± 0.0	3.2 ± 3.9	-
Fimbul	F2	02/01/19	110	100	0.0 ± 0.0	-	26.5 ± 0.1	0.1 ± 0.1	0.0 ± 0.1	0.0 ± 0.0	0.5 ± 2.1	48.6 ± 11.5
Fimbul	F3	03/01/19	63	75	0.0 ± 0.0	0.0 ± 0.0	26.0 ± 0.3	0.7 ± 0.3	1.2 ± 0.5	0.0 ± 0.0	1.8 ± 0.6	18.8 ± 1.1
Fimbul	F4	20/02/19	20	40	0.2 ± 0.2	0.2 ± 0.1	20.2 ± 1.9	3.7 ± 2.0	8.7 ± 0.6	0.3 ± 0.1	2.3 ± 0.5	11.7 ± 0.6
AP Average	**AP**		**23 ± 8**	**45 ± 9**	**0.8 ± 0.2**	**0.3 ± 0.1**	**24.9 ± 0.6**	**2.5 ± 1.7**	**1.1 ± 0.8**	**0.1 ± 0.1**	**0.6 ± 0.2**	**19.8 ± 16.5**
Antarctic Peninsula	AP1	09/01/19	23	35	0.6 ± 0.1	0.2 ± 0.1	25.6 ± 1.4	2.6 ± 0.7	1.4 ± 0.4	0.2 ± 0.1	0.5 ± 0.4	14.1 ± 0.4
Antarctic Peninsula	AP2	09/01/19	30	50	0.7 ± 0.1	0.2 ± 0.1	25.9 ± 1.0	1.0 ± 1.1	0.8 ± 0.2	0.1 ± 0.0	0.8 ± 1.1	6.8 ± 1.1
Antarctic Peninsula	AP3	09/01/19	15	50	1.1 ± 0.0	0.3 ± 0.1	24.7 ± 0.3	3.2 ± 2.5	1.4 ± 1.5	0.1 ± 0.1	0.4 ± 1.4	38.4 ± 1.2
LCIS Average	**LCIS**		**14 ± 6**	**29 ± 9**	**0.7 ± 0.4**	**0.2 ± 0.1**	**16.4 ± 4.7**	**8.2 ± 4.9**	**8.1 ± 4.9**	**0.6 ± 0.3**	**1.0 ± 0.2**	**14.7 ± 2.9**
Larsen C	L1	22/01/19	8.5	33	1.3 ± 0.1	0.4 ± 0.1	21.8 ± 0.1	2.0 ± 0.1	2.3 ± 0.3	0.2 ± 0.1	1.2 ± 0.1	11.2 ± 0.3
Larsen C	L2	20/01/19	14	25	0.4 ± 0.3	0.2 ± 0.2	13.7 ± 5.0	8.6 ± 4.8	7.8 ± 4.7	0.6 ± 0.4	0.9 ± 0.8	15.2 ± 1.0
Larsen C	L3	11/01/19	7	50	0.9 ± 0.1	0.2 ± 0.1	23.1 ± 0.2	2.2 ± 0.1	1.3 ± 0.8	0.1 ± 0.1	0.6 ± 0.6	17.7 ± 0.3
Larsen C	L4	14/01/19	24	22	0.5 ± 0.5	0.1 ± 0.1	12.1 ± 2.5	12.8 ± 2.1	10.9 ± 2.2	0.9 ± 0.2	0.9 ± 0.3	13.9 ± 0.2
Larsen C	L5	15/01/19	10	25	0.1 ± 0.0	0.4 ± 0.2	12.0 ± 1.9	10.9 ± 2.3	9.6 ± 1.7	0.8 ± 0.1	0.9 ± 0.3	13.7 ± 0.2
Larsen C	L6	13/01/19	17.5	30	0.7 ± 0.5	0.2 ± 0.1	15.1 ± 2.1	8.4 ± 2.1	8.0 ± 1.9	0.4 ± 0.1	1.0 ± 0.3	20.4 ± 0.3
Larsen C	L7	22/01/19	8.5	25	1.0 ± 1.1	0.2 ± 0.1	14.7 ± 4.1	11.1 ± 1.8	13.5 ± 3.4	0.8 ± 0.2	1.2 ± 0.3	14.8 ± 0.3
Larsen C	L8	23/01/19	22.5	35	0.3 ± 0.0	0.2 ± 0.0	12.2 ± 2.2	12.9 ± 4.5	12.4 ± 3.2	0.8 ± 0.3	1.0 ± 0.4	16.0 ± 0.5
Larsen C	L9	19/01/19	12.5	20	0.5 ± 0.4	0.2 ± 0.1	20.2 ± 4.3	5.8 ± 3.3	6.6 ± 5.1	0.5 ± 0.3	1.1 ± 1.0	11.0 ± 0.9
Larsen C	L10	24/01/19	14	20	0.7 ± 0.3	0.2 ± 0.1	18.2 ± 5.4	8.7 ± 3.7	10.6 ± 4.9	0.7 ± 0.3	1.2 ± 0.6	13.0 ± 0.6
WG Average	**WG**		**20 ± 0**	**90 ± 14**	**0.2 ± 0.2**	**0.1 ± 0.1**	**28.8 ± 2.4**	**0.4 ± 0.3**	**2.0 ± 0.9**	**0.1 ± 0.0**	**5.6 ± 0.7**	**4.1 ± 0.6**
Weddell Gyre	WG1	14/02/19	20	100	0.2 ± 0.2	0.1 ± 0.1	26.7 ± 0.5	0.4 ± 0.3	2.3 ± 0.8	0.1 ± 0.0	5.1 ± 0.7	4.5 ± 0.7
Weddell Gyre	WG2	15/02/19	20	80	0.4 ± 0.1	0.1 ± 0.1	30.2 ± 0.8	0.3 ± 0.4	2.0 ± 1.0	0.1 ± 0.1	6.1 ± 1.3	3.7 ± 1.5

https://doi.org/10.5194/bg-2021-122
Preprint. Discussion started: 17 May 2021
© Author(s) 2021. CC BY 4.0 License.

Biogeosciences
Discussions
Open Access
EGU

617

Table 2. Euphotic zone-integrated rates and averages at each station occupied in the Weddell Sea in summer 2018/2019. Values shown are averages ± 1 SD (n ≥ 2). "-" indicates no available data and the values shown in italics (i.e., purea) were estimated rather than measured (see text for details).

Station position	Station	[PON] (µM)	C:N ratio	NPP (mmol m^{-2} d^{-1})	ρNO_3^- (mmol m^{-2} d^{-1})	ρNH_4^+ (mmol m^{-2} d^{-1})	purea (mmol m^{-2} d^{-1})	$V_{NO_3^-}$ (µmol m^{-2} d^{-1})	f-ratio$_{(excluding\ urea)}$	f-ratio$_{(including\ urea)}$
FIS Average	**FIS**	**0.8 ± 0.9**	**16.5 ± 8.8**	**27.5 ± 26.6**	**3.7 ± 1.0**	**0.8 ± 0.4**	***0.5 ± 0.4***	**0.3 ± 0.2**	**0.80 ± 0.10**	**0.73 ± 0.09**
Fimbul	F1	0.3 ± 0.2	21.6 ± 3.7	4.9 ± 0.0	3.8 ± 0.0	0.4 ± 0.0	*0.3 ± 0.0*	-	0.91	0.84
Fimbul	F2	0.2 ± 0.0	26.3 ± 12.6	20.8 ± 0.2	2.4 ± 0.0	0.8 ± 0.0	*0.07 ± 0.0*	-	0.75	0.70
Fimbul	F3	0.4 ± 0.2	8.8 ± 3.0	56.9 ± 0.6	4.8 ± 0.1	1.2 ± 0.0	*0.5 ± 0.0*	0.2 ± 0.0	0.80	0.74
Fimbul	F4	2.1 ± 0.6	9.4 ± 0.5	28.3 ± 0.4	3.9 ± 0.0	1.9 ± 0.0	*0.9 ± 0.0*	0.4 ± 0.0	0.68	0.63
AP Average	**AP**	**1.1 ± 0.3**	**8.3 ± 2.5**	**26.6 ± 33.5**	**3.4 ± 1.4**	**3.8 ± 2.0**	***0.5 ± 0.2***	**0.0 ± 0.1**	**0.52 ± 0.17**	**0.48 ± 0.16**
Antarctic Peninsula	AP1	1.3 ± 0.1	6.1 ± 1.4	3.1 ± 0.1	1.8 ± 0.1	2.6 ± 0.0	*0.4 ± 0.0*	0.0 ± 0.0	0.41	0.38
Antarctic Peninsula	AP2	0.8 ± 0.3	7.8 ± 2.7	11.8 ± 0.2	4.0 ± 0.2	2.1 ± 0.0	*0.4 ± 0.0*	0.0 ± 0.0	0.72	0.67
Antarctic Peninsula	AP3	1.3 ± 0.2	11.0 ± 2.1	65.0 ± 0.1	4.4 ± 0.0	5.8 ± 0.0	*0.8 ± 0.0*	0.1 ± 0.0	0.43	0.40
LCIS Average	**LCIS**	**2.4 ± 0.8**	**7.4 ± 1.9**	**28.6 ± 21.3**	**2.2 ± 1.1**	**2.6 ± 1.3**	**0.6 ± 0.3**	**0.5 ± 0.8**	**0.50 ± 0.09**	**0.47 ± 0.08**
Larsen C	L1	1.5 ± 0.3	10.0 ± 3.4	2.2 ± 0.1	1.5 ± 0.0	1.4 ± 0.0	0.2 ± 0.0	0.7 ± 0.0	0.52	0.50
Larsen C	L2	3.1 ± 0.5	6.3 ± 1.7	47.8 ± 0.5	1.5 ± 0.1	3.3 ± 0.0	0.8 ± 0.0	0.3 ± 0.0	0.54	0.51
Larsen C	L3	2.6 ± 0.8	5.8 ± 1.4	32.0 ± 0.1	2.5 ± 0.0	3.3 ± 0.0	0.3 ± 0.0	2.9 ± 0.0	0.42	0.41
Larsen C	L4	1.0 ± 0.2	8.0 ± 0.5	32.2 ± 1.0	1.9 ± 0.1	2.1 ± 0.0	0.2 ± 0.0	-	0.49	0.48
Larsen C	L5	3.1 ± 0.6	7.4 ± 1.9	61.0 ± 0.7	4.7 ± 0.0	3.1 ± 0.0	0.9 ± 0.0	0.1 ± 0.0	0.60	0.56
Larsen C	L6	2.4 ± 0.5	9.2 ± 5.3	25.9 ± 1.5	2.4 ± 0.1	2.2 ± 0.1	0.7 ± 0.0	0.4 ± 0.0	0.53	0.49
Larsen C	L7	1.5 ± 0.7	8.2 ± 1.1	55.9 ± 1.0	3.1 ± 0.0	3.8 ± 0.1	1.1 ± 0.0	0.0 ± 0.0	0.45	0.42
Larsen C	L8	3.3 ± 0.3	8.2 ± 1.3	17.3 ± 0.4	2.3 ± 0.0	4.8 ± 0.1	0.9 ± 0.0	0.4 ± 0.0	0.32	0.30
Larsen C	L9	2.9 ± 0.2	3.4 ± 4.1	9.7 ± 1.3	2.0 ± 0.1	1.2 ± 0.0	0.6 ± 0.0	0.5 ± 0.0	0.63	0.57
Larsen C	L10	2.7 ± 1.1	7.1 ± 0.4	1.8 ± 0.0	0.5 ± 0.0	0.6 ± 0.0	0.2 ± 0.0	0.1 ± 0.0	0.46	0.42
WG Average	**WG**	**0.7 ± 0.3**	**12.3 ± 1.8**	**31.6 ± 31.3**	**3.2 ± 0.1**	**2.0 ± 0.2**	***0.5 ± 0.1***	**9.0 ± 6.8**	**0.54 ± 0.10**	**0.48 ± 0.12**
Weddell Gyre	WG1	0.5 ± 0.2	13.6 ± 7.7	53.7 ± 0.2	3.3 ± 0.0	2.1 ± 0.0	0.6 ± 0.0	13.8 ± 0.2	0.47	0.39
Weddell Gyre	WG2	0.9 ± 0.3	11.0 ± 7.5	9.5 ± 0.4	3.1 ± 0.0	1.8 ± 0.0	*0.4 ± 0.0*	4.2 ± 0.0	0.61	0.56

https://doi.org/10.5194/bg-2021-122
Preprint. Discussion started: 17 May 2021
© Author(s) 2021. CC BY 4.0 License.

4. Discussion

Across the Weddell Sea in summer 2019, the euphotic zone-integrated rates of NPP and N uptake were generally lower at the OOZ stations than the CCSZ stations, with the highest depth-specific uptake rates observed in surface waters at LCIS (Figure 6a-d; Table 2). The few studies that have previously measured summertime rates of NPP and N uptake in the Weddell Sea reported similar results, with rates in the marginal ice zone (MIZ) and CCSZ that were up to five-times higher than in the OOZ (El-Sayed and Taguchi 1981; Smith and Nelson 1990; Park et al. 1999). The summertime CCSZ of the Weddell Sea can thus be broadly characterised as a highly productive region with elevated biomass accumulation driven by increased water-column stratification and iron-replete conditions, both the result of sea-ice melt (Semeneh et al. 1998; Lannuzel et al. 2008; Klunder et al. 2011). However, we observed considerable variability in the biogeochemical rates measured within each region of the Weddell Sea, particularly at LCIS; we examine the possible drivers of the inter- and intraregional differences below.

4.1. Drivers of NPP and N uptake in the Weddell Sea

Light and water column stability: Surface waters throughout the study region were generally well stratified, with MLDs ranging from 7 to 30 m, except at the early-summer FIS stations where the MLD ranged from 63 to 135 m (Table 1). These deep MLDs coincided with elevated concentrations of sea-ice, while the shallowest MLDs observed at LCIS occurred in relatively ice-free surface waters. Average euphotic zone rates of NPP and ρNO_3^- generally varied with the depth of the mixed layer and Z_{eu} at all stations – they were highest (lowest) at the stations where Z_{eu} was shallowest (deepest) (Figure 10a-b), implicating light as a major control on NPP and ρNO_3^-. At LCIS, however, the euphotic zone was shallow at all stations (<50 m, average Z_{eu} of 28.5 ± 9 m), yet NPP and ρNO_3^- varied by over an order of magnitude (Table 2). We observed a positive relationship between the LCIS rates and SST, with NPP and ρNO_3^- increasing at higher SSTs, the latter indicative of increased water column stratification (Figure 10d; see below).

Throughout the region, the average euphotic zone rates of ρNH_4^+ and ρurea also varied with Z_{eu} (Figure 10c), suggesting that these processes were light dependent too. This is unexpected, as the energy requirement associated with NH_4^+ and urea assimilation is low (El-Sayed and Taguchi 1981; Dortch 1990; Jacques 1991; Goeyens et al. 1995; Priddle et al. 1998). The stations with the deepest Z_{eu} were also characterized by low concentrations of regenerated N (Figures 3a-b and 10c), leading us to conclude that ρNH_4^+ and ρurea were predominantly constrained by the availability of regenerated N rather than by light. This conclusion is supported by the observed increase in ρNH_4^+ and ρurea towards the base of the euphotic zone at stations with elevated regenerated N concentrations (e.g., station L8; Figures 6c-d, g-h, and k-l, and 10c).

The lowest regenerated N concentrations occurred at the stations with the lowest rates of NPP and ρNO_3^-, and the highest NO_3^- concentrations (e.g., station F1). This is probably because NH_4^+ and urea tend to accumulate only when biomass (and productivity) is sufficiently high to support elevated rates of heterotrophic activity (Semeneh et al. 1998). At the stations with low POC and PON concentrations, remineralisation rates were likely also low, limiting the flux of NH_4^+ and urea and driving low rates of ρNH_4^+ and ρurea. At the stations where NH_4^+ and urea concentrations were elevated, rates of ρNH_4^+ and ρurea increased with depth, along with a decrease in NPP and

https://doi.org/10.5194/bg-2021-122
Preprint. Discussion started: 17 May 2021
© Author(s) 2021. CC BY 4.0 License.

658 ρNO_3^- (e.g., station L8). These observations further demonstrate the control of light on NPP and ρNO_3^-, and
659 substrate availability on ρNH_4^+ and ρurea. That said, it is unlikely that the variability in NPP and N uptake among
660 the stations was driven by light and nutrient availability alone, and we hypothesize that hydrography, iron
661 availability, and phytoplankton community composition also played a role.
662

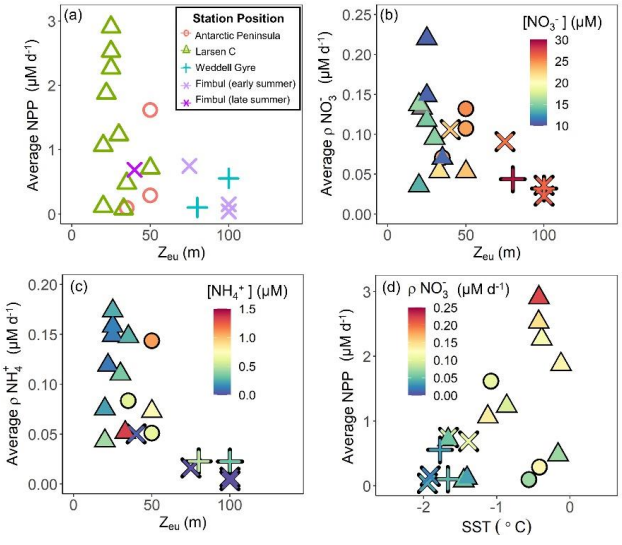

663
664 **Figure 10.** Euphotic zone-averaged rates of (a) NPP, (b) ρNO_3^- and (c) ρNH_4^+ versus Z_{eu}, and (d) NPP versus SST
665 at each station. The symbols in panels (b) and (c) are coloured by nutrient concentration and in panel (d), by ρNO_3^-
666

667 At LCIS, the stations closest to the ice shelf were characterised by low SSTs and low rates of NPP and N uptake
668 (stations L1 and L3; Figures 1 and 11a; Table 2). The low SSTs can be attributed either to the formation of sea-
669 ice or to the upwelling of WW along the ice shelf. Sea-ice formation, in addition to decreasing SST, also increases
670 the salinity of ASW due to brine rejection (Brennecke 1921; Mosby 1934; Gill 1973). While the salinity of ASW
671 at the low-SST stations was indeed elevated, the oxygen concentrations were relatively low (≤ 300 μM, which is
672 below saturation; Figure 11c and d). In surface waters and sea-ice, oxygen is typically saturated as it rapidly
673 equilibrates with the atmosphere (Gleitz et al. 1995). Sea-ice formation should not, therefore, drive a notable
674 change in the oxygen content of ASW. The low oxygen concentrations at stations L1 and L3 were contiguous
675 with those in the underlying WW (Figure 11d), leading us to conclude that the cool, saline waters along the ice-
676 shelf front indicate recent upwelling of WW. Such upwelling could temporarily inhibit productivity by decreasing
677 the stability of the water column, thereby mixing phytoplankton below the euphotic zone. This mechanism can
678 explain the low uptake rates and weak nutrient depletions observed at the low-SST stations.
679

680 Relatively cold, saline surface waters have previously been observed at the ice-edge off Larsen A and B Ice
681 Shelves ~~and shown to hinder~~ NPP (Cape et al. 2014). Here, the dense surface waters were surmised to result either
682 from offshore wind stress at the inshore region that induced localised mixing, or ~~from the advection of surface~~
683 ~~waters offshore~~ by coastal upwelling. Both mechanisms would decrease water column stability, and by extension,
684 productivity. Cape et al. (2014) observed an increase in NPP with distance from the coast at Larsen A and B, a

https://doi.org/10.5194/bg-2021-122
Preprint. Discussion started: 17 May 2021
© Author(s) 2021. CC BY 4.0 License.

trend that we did not observe, likely because of the proximity of our LCIS stations to the ice shelf (within 75 km for all stations). Instead, our rates of NPP and N uptake were positively coupled with SST at the ice-edge (Figure 10d). We propose that surface SST at LCIS can be used as an indicator of water-mass age, with cooler SSTs indicating newly-upwelled WW and warmer SSTs designating older surface waters that have had time to absorb heat from the atmosphere. The higher rates of NPP and N uptake in the warm surface waters occur because phytoplankton have experienced favourable growing conditions for an extended period, resulting in the accumulation of biomass. By contrast, persistent localised upwelling along LCIS inhibits productivity in the adjacent surface waters, with implications for the spatial distribution of biomass and organic carbon export.

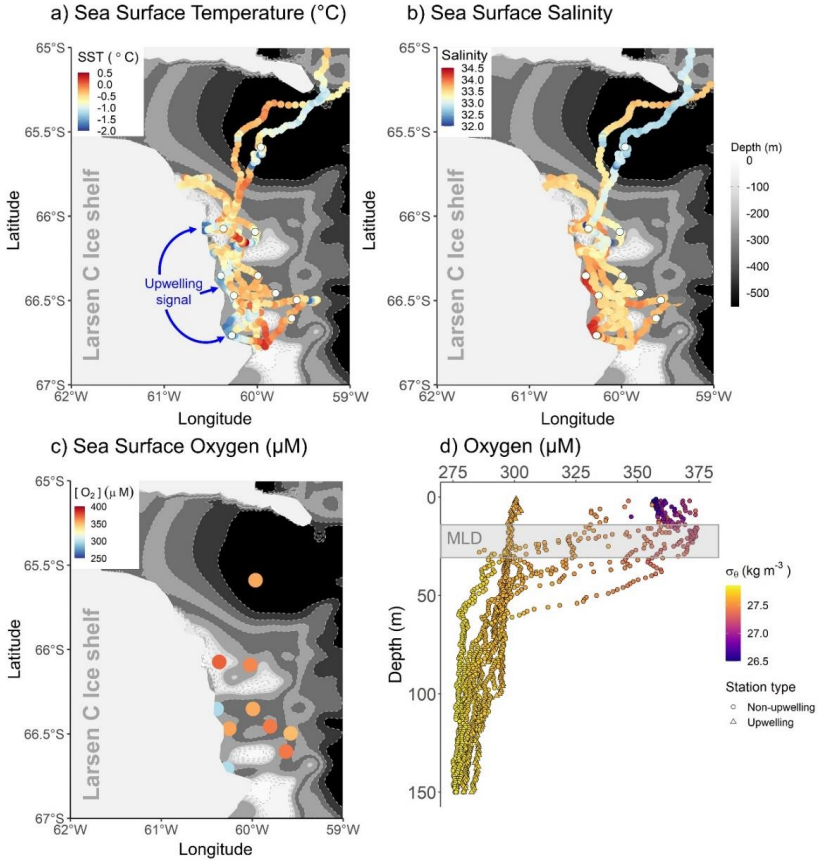

Figure 11. Maps of (a) SST, (b) sea surface salinity, and (c) surface oxygen concentrations, and (d) depth profiles of oxygen concentrations in the region of LCIS at the time of sampling. SST and salinity data were acquired from the underway (~7 m inflow) ferrybox, while the oxygen concentrations were measured via the oxygen sensor on the CTD profiler, calibrated against discrete seawater samples measured for dissolved oxygen by Winkler titration (Carpenter 1965; Grasshoff et al. 1983; Hutchinson et al. 2020)(Carpenter 1965; Grasshoff, Kremling, and Ehrhard 1983)(Carpenter 1965; Grasshoff, Kremling, and Ehrhard 1983)(Carpenter 1965; Grasshoff, Kremling, and Ehrhard 1983). The symbols in panel (d) are coloured by potential density (σ_θ), with the circles indicating the non-upwelling stations and the triangles the upwelling stations. The grey box in panel (d) indicates the average mixed layer depth (MLD) across the stations at LCIS. The bathymetry data in panels (a-c) were taken from ETOPO1 (NOAA National Geophysical Data Center 2009).

https://doi.org/10.5194/bg-2021-122
Preprint. Discussion started: 17 May 2021
© Author(s) 2021. CC BY 4.0 License.

706 *Nutrient and iron conditions in Weddell Sea surface waters*: Across our sampling region, ASW was depleted in
707 NO_3^-, $Si(OH)_4$ and PO_4^{3-} relative to the underlying WW, with the greatest nutrient depletion occurring at LCIS
708 and at FIS in late summer (Figure 4a-c). Under iron-replete conditions, diatoms consume Si:N:P in an approximate
709 ratio of 1:1:0.07 (Ragueneau et al. 2000; Hutchins and Bruland 1998; Takeda 1998; Mosseri et al. 2008), while
710 under iron-limitation, they increase their uptake of Si and decrease that of P relative to N, consuming nutrients in
711 a ratio of ≥2:1:0.09 (Arrigo et al. 1999; Finkel et al. 2006; Green and Sambrotto 2006; Weber and Deutsch 2010;
712 Martiny et al. 2013; Mosseri et al. 2008), with Si:N uptake ratios as high as 8:1 occurring when iron is very low
713 (Franck et al. 2000; Brzezinski et al. 2003). The Si:N:P depletion ratios (more correctly, $Si(OH)_4$:NO_3^-:PO_4^{3-}
714 depletion ratios) estimated in our study suggest that the AP and LCIS stations were characterised by iron-replete
715 conditions (ratio of 0.9:1:0.06) while the phytoplankton community at the FIS and WG stations experienced iron
716 limitation (ratios of 3.6:1:0.15; Figures 4d and 4e; Table 1).
717
718 High iron concentrations have previously been measured in surface waters in the CCSZ and northern Weddell Sea
719 (7 nM; Lannuzel et al. 2008; De Jong et al. 2012). Iron is supplied to the mixed layer in these regions via sea-ice
720 melt, ice shelf melt, continental runoff, vertical and lateral advection, and resuspension of continental shelf
721 sediments (Lannuzel et al. 2008; De Jong et al. 2012; Klunder et al. 2014). In contrast, the central WG is iron
722 limited as iron is supplied to surface waters mainly by wind-induced vertical mixing (Hoppema et al. 2015).
723 During our sampling, sea-ice concentrations were high at the WG stations, which would have dampened the effect
724 of wind stress on surface waters and thus hindered vertical mixing. At FIS in early summer, iron is expected to be
725 replete as phytoplankton will not have had sufficient time to exhaust the surface reservoir. Here, the sea-ice
726 concentrations were elevated, and the mixed layers were deep such that light, rather than iron, likely limited
727 phytoplankton growth. Light-limited diatoms have been observed to consume Si:N:P in a ratio similar to that
728 reported under conditions of iron depletion (Brzezinski 1985). By late summer at FIS, the sea-ice had completely
729 melted, which should have further alleviated iron limitation, yet the $Si(OH)_4$:NO_3^- depletion ratios were
730 characteristic of iron-deplete diatoms (average of 2.3 ± 0.5). These apparently high Si:N depletion ratios may be
731 due to our not accounting for regenerated N uptake. At FIS in late summer, NH_4^+ supported 32% of N uptake;
732 accounting for this N source decreases the Si:N depletion ratio to 1.4:1, which is closer to that expected for iron-
733 replete diatoms. While some diatom growth was likely also supported by urea, which would further decrease the
734 Si:N depletion ratio, it is nonetheless plausible that the diatoms at F4 were beginning to experience iron-limitation
735 as the station was sampled late in the season.
736
737 Accounting for regenerated N uptake greatly alters the Si:N depletion ratios, particularly at LCIS, and provides
738 insights into the dominant phytoplankton groups that were active in the mixed layer, both prior to and at the time
739 of sampling. From the Si:NO_3^- depletion ratio at LCIS, we infer that *P. antarctica* predominantly consumed
740 regenerated sources of N. Our reasoning relies on that fact that under favourable nutrient and light conditions,
741 diatoms will rely near-exclusively on NO_3^- (Lomas and Glibert 1999), such that the average Si:NO_3^- depletion
742 ratio at LCIS of 1.0 ± 0.2 can be attributed entirely to this phytoplankton group. When total N uptake is considered,
743 the Si:N depletion ratios decrease to 0.3 ± 0.1, indicating the consumption of three-times more N than $Si(OH)_4$,
744 which we attribute to regenerated N uptake by *P. antarctica*. Indeed, this phytoplankton group is known to
745 preferentially consume NH_4^+ when it is available due to the lower energy (El-Sayed and Taguchi 1981; Dortch

https://doi.org/10.5194/bg-2021-122
Preprint. Discussion started: 17 May 2021
© Author(s) 2021. CC BY 4.0 License.

1990; Jacques 1991; Goeyens et al. 1995; Priddle et al. 1998) and iron requirements (Stefels and Van Leeuwe 1998) associated with NH_4^+ assimilation. By contrast, diatoms are NO_3^- specialists that can outcompete other phytoplankton for this N source (Malone 1980; Fawcett and Ward 2011). They have even been observed to consume NO_3^- under iron-deplete conditions, which is possible because of their low iron requirement relative to that of other phytoplankton groups (Marchetti and Maldonado 2016; Marchetti and Cassar 2009).

We can also use the NO_3^-:PO_4^{3-} depletion ratios to better understand the iron conditions and the relative importance of *P. antarctica* versus diatoms in generating the observed nutrient depletion ratios. *P. antarctica* are known to consume NO_3^- and PO_4^{3-} in a ratio of ~20:1, while for iron-replete diatoms, this ratio is <14:1 (Arrigo et al. 1999; Smith and Asper 2001; Garcia et al. 2018). At LCIS, the NO_3^-:PO_4^{3-} depletion ratio averaged 14.7 ± 2.9, consistent with a dominant role for iron-replete diatoms. However, variability in the NO_3^-:PO_4^{3-} depletion ratios was observed among the LCIS stations (with ratios ranging from 11 to 20), which we attribute to local variations in phytoplankton community composition. At stations where large diatoms were dominant (e.g., L10, where diatoms contributed 6.47 pg C L^{-1} to biomass while *P. antarctica* only contributed 0.07 pg C L^{-1}; Leblanc et al. 2012; Mathot et al. 2000), the NO_3^-:PO_4^{3-} depletion ratios were low (13.0 ± 0.6). In contrast, at the stations where *P. antarctica* were numerically dominant (e.g., L6; where *P. antarctica* constituted 90% of the phytoplankton population) and contributed more to biomass (0.17 pg C L^{-1}), elevated NO_3^-:PO_4^{3-} depletion ratios were measured (20.4 ± 0.3; Figure 9d-f; Table 1). Furthermore, high rates of NH_4^+ uptake were measured at LCIS, equivalent to and at times greater than the coincident NO_3^- uptake rates. *P. antarctica* has been observed to preferentially consume NH_4^+, while diatoms will consume NO_3^- if iron is available (Probyn and Painting 1985; Lomas and Glibert 1999; Glibert et al. 2016). The relative contribution of diatoms versus *P. antarctica* to biomass thus appears to control the nutrient depletion ratios on a variety of scales across the Weddell Sea.

Drivers of phytoplankton community composition: Phytoplankton community composition and the variations therein have implications for the biological pump, both directly (diatoms sink more rapidly than smaller and/or non-ballasted phytoplankton; Treguer and Jacques 1992; De Baar et al. 2005; Boyd et al. 2007) and indirectly (NO_3^- consumption is quantitatively related to carbon export; Dugdale and Goering 1967; Eppley and Peterson 1979). Above, we have discussed the biogeochemical evidence for the dominance of one phytoplankton group over another in driving productivity and nutrient consumption. Below, we discuss the processes that may have resulted in the dominance of *P. antarctica* over diatoms at LCIS, and vice versa at the other Weddell Sea stations.

At LCIS, a coastal sensible heat polynya persisted throughout the sampling period. The opening of such polynyas along the eastern AP is linked to the occurrence of warm, föhn winds that originate over the continent and blow over the AP, influencing the coastal north-western Weddell Sea (Cape et al. 2014). Föhn winds drive the offshore movement of sea-ice, which initiates the opening of polynyas that persist because the winds are warm, thus hindering the formation of new sea-ice (Cape et al. 2014). The development of coastal sensible heat polynyas results in relatively deep mixed layers and a weakly stratified water column. The polynya at LCIS opened in late November, approximately two months prior to our sampling. At this time (i.e., the beginning of the growing season), motile *P. antarctica* cells likely dominated the phytoplankton community as *P. antarctica* are low-light specialists compared to other Antarctic phytoplankton (Goffart et al. 2000; Delmont et al. 2014). This notion is

https://doi.org/10.5194/bg-2021-122
Preprint. Discussion started: 17 May 2021
© Author(s) 2021. CC BY 4.0 License.

supported by the low phytoplankton cell counts (for both flow cytometry and net samples) and high relative abundance of *P. antarctica* compared to diatoms at the stations along the ice shelf where WW had recently upwelled (e.g., L3; Figure 9a, d and e). As the mixed layer shoaled and light limitation was alleviated, a diatom bloom would have been initiated and *P. antarctica* colony formation would have occurred (Schoemann et al. 2005). Indeed, the presence of *P. antarctica* (as colonies) and diatoms (as chains) at the time of our sampling in January is evidence that the water column was well stratified (Goffart et al. 2000). As the season progressed, diatoms would have outcompeted *P. antarctica* and come to dominate the phytoplankton community. At the stations sampled later in the season (e.g., L10; Figure 9e), the relative abundance of diatoms versus *P. antarctica* was greater than at the stations sampled two weeks earlier (e.g., L5; Figure 9e). Diatoms have a lower iron and higher light requirement than *P. antarctica* and thus tend to thrive once the *P. antarctica* bloom is over, when the water column has stratified and they can utilize the lower concentrations of residual iron (Strzepek et al. 2011). That said, iron is likely perennially high at LCIS as it is near-continuously supplied to surface waters in summer by sea-ice melt and upwelling of WW along the ice shelf (Klunder et al. 2014). The elevated iron concentrations would allow the diatoms to grow rapidly on the available NO_3^- once the mixed layer had shoaled enough to alleviate light limitation.

Throughout the rest of the Weddell Sea, diatoms dominated the phytoplankton community. Here, we hypothesize that at the beginning of the growing season, melting sea-ice alleviated light- and, to a lesser extent, iron limitation, providing favourable conditions for diatom growth. At the same time, the generally lower iron concentrations characteristic of open Weddell Sea waters may have selected against *P. antarctica*. Previous studies conducted in the Ross Sea observed large diatom blooms associated with the receding ice-edge and concluded that bloom formation was favoured by the rapid stabilization of the water column from meltwater inputs (Goffart et al. 2000; Sedwick et al. 2000). Regions of the Weddell Sea that undergo rapid stratification due to sea-ice melt will likely also experience large diatom blooms. We thus conclude that the dominance of diatoms over *P. antarctica* at the non-LCIS stations was influenced by local hydrodynamic processes that induce water column stability and allow access to sufficient light (e.g., in areas of recent sea-ice melt). By contrast, *P. antarctica* dominates under conditions of low light, such as the deep mixed layers that initially characterize coastal polynyas. Eventually, diatoms will succeed *P. antarctica* in these polynyas once conditions become favourable for their growth.

4.2. Carbon export potential across the Weddell Sea

Previous f-ratio estimates for the summertime Weddell Sea range from 0.18 to 0.83 (Koike et al. 1986; Rönner et al. 1983; Nelson et al. 1987; Smith and Nelson 1990; Goeyens 1991; Goeyens et al. 1995). Using equations 4a and 4b, we calculate euphotic zone-integrated f-ratios that range from 0.32 to 0.91 (excluding urea uptake) and 0.30 to 0.84 (including urea uptake). The lowest f-ratios were observed at LCIS ($\text{f-ratio}_{(\text{excluding urea})} = 0.50 \pm 0.09$ and $\text{f-ratio}_{(\text{including urea})} = 0.47 \pm 0.08$) and the highest at FIS ($\text{f-ratio}_{(\text{excluding urea})} = 0.78 \pm 0.1$ and $\text{f-ratio}_{(\text{including urea})} = 0.73 \pm 0.09$) (Figure 8; Table 2). We note that urea uptake may have been stimulated at the stations where it was measured given the quantity of ^{15}N-urea added (0.1 µM) relative to the ambient urea concentrations (average of 0.2 ± 0.1 µM; Figure S2; section S3 in the Supplemental Information); if so, regenerated production could be overestimated at all stations since we applied the average measured contribution of urea-to-total-N uptake (8 ± 6%) to the stations at which ρurea was not measured (equation 7). The f-ratio estimates excluding and including

https://doi.org/10.5194/bg-2021-122
Preprint. Discussion started: 17 May 2021
© Author(s) 2021. CC BY 4.0 License.

urea uptake thus represent an upper and lower bound on the fraction of potentially exportable carbon. That said, accounting for urea uptake decreased the average f-ratio from 0.57 ± 0.15 to 0.52 ± 0.14 which is minor (Figure 8; Table 2).

Estimates of the f-ratio and carbon export potential can be further complicated by euphotic zone nitrification, which supplies regenerated rather than new NO_3^- to the euphotic zone. Failing to account for this regenerated N flux leads to an overestimation of carbon export potential (Yool et al. 2007; Mdutyana et al. 2020). At all the stations sampled, the euphotic zone rates of $V_{NO_2^-}$ were low (undetectable to 9.5 nM d^{-1}; Figure 7b) and correcting the f-ratio for euphotic zone nitrification (equation 4) had a minimal effect on our estimates (average decrease of 2 ± 6%). The largest decrease was observed at WG1 where the highest euphotic zone-integrated rates of $V_{NO_2^-}$ were measured (f-ratio$_{(excluding\ urea)}$ decreased from 0.6 to 0.47 and f-ratio$_{(including\ urea)}$ decreased from 0.49 to 0.39; Table 2).

The low rates of euphotic zone nitrification are consistent with the previous (limited) data available for the summertime OOZ and CCSZ of the Southern Ocean. For example, Mdutyana et al. (2020) measured euphotic zone rates of $V_{NO_2^-}$ and NH_4^+ oxidation in summer at FIS and in the Antarctic Zone just north of the WG (56°S 0°E) that were below detection. Summertime studies of euphotic zone NH_4^+ oxidation in the Ross and Scotia Seas reported similarly low rates of 6-8.9 nM d^{-1} and 0.4-5.8 nM d^{-1}, respectively (Olson 1981). We conclude that, as expected, the high-light and generally low-NH_4^+ conditions of the summertime Weddell Sea inhibited euphotic zone nitrification (Horrigan 1981; Olson 1981; Guerrero and Jones 1996; Merbt et al. 2012; Qin et al. 2014), and that the slow growing nitrifiers were likely also outcompeted by phytoplankton for any available NH_4^+ (Ward 1985; 2005; Smith et al. 2014; Zakem et al. 2018). Classifying NO_3^- uptake as new production and equating it to carbon export potential thus seems reasonable for the summertime Weddell Sea.

Although the highest f-ratios were estimated for the FIS stations, the highest rates of ρNO_3^- were observed at LCIS and along the AP (Figure 8; Table 2). FIS was thus characterised by the highest carbon export potential relative to NPP, while the N cycle data imply that the absolute carbon export flux was highest at LCIS and the AP. The maximum extent of nutrient depletion was also observed at LCIS (NO_3^- depletion of 57-428 mmol m^{-2} and PO_4^{3-} depletion of 5.8-18.7 mmol m^{-2}). Assuming Redfield C:N and C:P stoichiometry of 6.63:1 and 106:1, respectively, the seasonal NO_3^- depletion equates to a carbon export flux of 0.4-2.8 mol C m^{-2} and the PO_4^{3-} depletion to 0.6-2.0 mol C m^{-2}. Alternately, multiplying ρNO_3^- by the length of time that the coastal polynya had been open (30 November until the date of sampling; Table 1) yields an estimate for net seasonal NO_3^- uptake of 59-428 mmol m^{-2} and carbon export flux of 0.4-2.8 mol C m^{-2} at LCIS, remarkably similar to the estimates derived from seasonal NO_3^- depletion. Our estimates are, however, lower than those previously measured in the CCSZ and MIZ of the Weddell Sea (e.g., estimates for January/February range from 2.4-4.9 mol C m^{-2}; Rönner et al. 1983; Hoppema et al. 2000; 2007). Given the high-light and nutrient- and iron-replete conditions at LCIS, one might thus have expected higher f-ratios and carbon export potential (i.e., NO_3^- depletion), raising the question of the possible limitations thereon.

https://doi.org/10.5194/bg-2021-122
Preprint. Discussion started: 17 May 2021
© Author(s) 2021. CC BY 4.0 License.

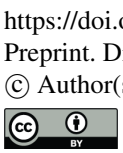

865 Throughout the Weddell Sea, NH_4^+ and urea uptake were coupled with substrate availability, while NO_3^- uptake
866 was not. Instead, NO_3^- uptake appeared to vary as a function of the ambient NH_4^+ concentration (Figure 12a). At
867 LCIS where NH_4^+ was elevated throughout the mixed layer at all stations, NO_3^- depletion, and therefore NO_3^-
868 uptake, decreased with increasing NH_4^+ (Figure 12b), which we attribute to NH_4^+ inhibition of NO_3^- uptake
869 (Goeyens et al. 1995). By contrast, at the other stations, NO_3^- depletion and ambient NH_4^+ concentration showed
870 a positive relationship, consistent with NO_3^--fuelled phytoplankton growth being followed by intense
871 remineralization and grazing, both of which can yield elevated NH_4^+ (Rönner et al. 1983; El-Sayed 1984; Semeneh
872 et al. 1998).
873

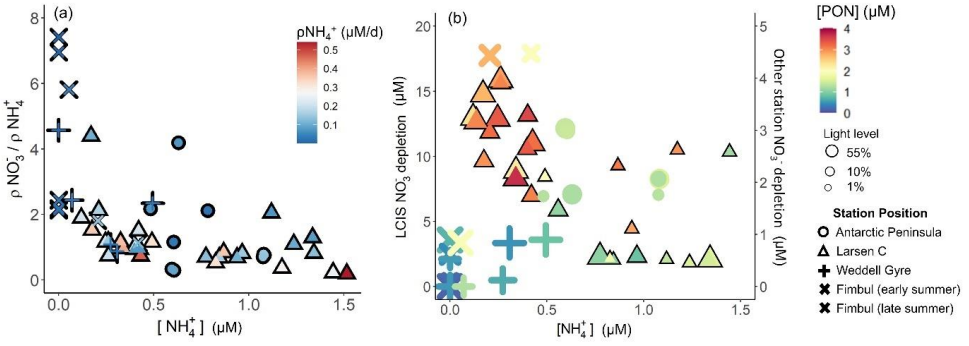

874

875 **Figure 12.** (a) NO_3^- uptake normalised to NH_4^+ uptake versus NH_4^+ concentration and b) NO_3^- depletion versus
876 NH_4^+ concentration. The symbols in panel (a) are coloured by NH_4^+ uptake rate and in panel (b) by PON
877 concentration. The symbol size in panel (b) represents the light level at which the samples were incubated. In
878 panel (b), NO_3^- depletion at LCIS corresponds with the primary y-axis and NO_3^- depletion at all other stations
879 corresponds with the secondary y-axis.
880

881 Previous studies conducted in MIZ and CCSZ of the Weddell Sea have shown that NH_4^+ concentrations ≥0.5 µM
882 can inhibit NO_3^- uptake, particularly by diatoms, resulting in phytoplankton preferentially consuming NH_4^+ over
883 NO_3^-. Goeyens et al. (1995) observed a Weddell Sea phytoplankton community dominated by diatoms prior to
884 NH_4^+ accumulation, but once surface waters became enriched in NH_4^+, diatom dominance ceased. The authors
885 concluded that diatom blooms were unable to develop despite the elevated NO_3^- because of the inhibitory effect
886 of NH_4^+, while non-siliceous phytoplankton species flourished because their preferred N source is NH_4^+. In our
887 study, although NH_4^+ inhibition of ρNO_3^- apparently occurred at LCIS, the rates of ρNO_3^- were on average as high
888 as ρNH_4^+ and were never zero (Table 2) – in other words, the high ambient NH_4^+ did not prevent NO_3^- uptake
889 even though it appears to have slowed it. We propose that the mixed community of diatoms and *P. antarctica*
890 present at the time of our sampling meant that diatoms were able to consume NO_3^- while *P. antarctica* consumed
891 the NH_4^+, preventing this reduced N form from accumulating to fully inhibitory concentrations. While the reliance
892 of *P. antarctica* on NH_4^+ over NO_3^- represents a missed opportunity for carbon export given that *P. antarctica* are
893 known to fix up to 50% more carbon than diatoms per mole of PO_4^{3-} consumed (Arrigo et al. 1999), that the
894 diatoms were able to proliferate in the face of elevated NH_4^+ may have partly compensated for this. Earlier in the
895 season when NH_4^+ concentrations were negligible, it is likely that the f-ratios at LCIS were >0.5 and comparable
896 to those at FIS, as observed at Larsen A and B in early summer (Goeyens et al. 1995; Cape et al. 2014). We
897 conclude that elevated NH_4^+ may have weakened carbon export potential at LCIS in January/February 2019

https://doi.org/10.5194/bg-2021-122
Preprint. Discussion started: 17 May 2021
© Author(s) 2021. CC BY 4.0 License.

Biogeosciences Discussions Open Access EGU

through its effect on whole-community NO_3^- uptake. Carbon export may have been further inhibited later in the season as NH_4^+ concentrations continued to increase following remineralisation of the phytoplankton bloom, coupled with the seasonal decrease in daylight that is expected to shift the phytoplankton community to proportionally higher NH_4^+ dependence (Glibert et al. 2016).

4.3. Broader biogeochemical implications at LCIS

LCIS is a region of deep-water formation, such that the biogeochemical properties of ASW influence those of MWDW and the bottom waters. Over the summer growing season, there was significant net depletion of nutrients from ASW. These nutrients were converted to organic matter (OM), which was then either consumed by zooplankton or exported out of the euphotic zone and decomposed by heterotrophic bacteria on the shelf and in the overlying waters. The on-shelf remineralisation of OM acts to increase the CO_2 and nutrient reservoir of WW and shelf waters (ISW and HSSW; both precursors of CDW). Some portion of this CO_2 ~~is effluxed~~ to the atmosphere when WW upwells along the ice shelf front, while the rest ~~will be mixed into~~ MWDW and eventually transferred to the bottom waters where it ~~will~~ be stored for hundreds of years (Ito et al. 2010). Biological activity and nutrient drawdown at LCIS, and the limitations thereon, thus affect the CO_2 and nutrient content of the bottom waters. The $Si(OH)_4$:NO_3^-:PO_4^{3-} ratio at depth at LCIS (average of 2:1:14 below 150 m) implicates diatoms as the main biological driver of the nutrient conditions in MWDW, and by extension the bottom waters, throughout the Weddell Sea. Although the dominance of *P. antarctica* in early and mid-summer does not appear to affect the nutrient properties of MWDW, it likely influences its CO_2 content. *P. antarctica* consume approximately twice as much carbon per PO_4^{3-} as diatoms, and the colonial forms have been observed to rapidly sink out of the water column, thereby transporting large quantities of carbon to depth (Arrigo et al. 2000; Ditullio et al. 2000). The dominance of *P. antarctica* at LCIS may thus be important for carbon storage in MWDW and the bottom waters.

As SSTs rise and sea-ice melts, a shift from *P. antarctica*- to diatom-dominated phytoplankton blooms is expected because diatoms flourish under conditions of high light and water column stratification (i.e., in areas of recent sea-ice melt) (Boyd and Doney 2002; Arrigo and van Dijken 2003; Petrou et al. 2016; Ferreira et al. 2020). Given the anomalously high carbon-to-nutrient content of *P. antarctica*, such a shift may negatively affect the export and storage of carbon in MWDW and the bottom waters. However, rising SSTs will also lead to increased glacial and ice shelf melt, further stratifying the adjacent water column and increasing the iron supply (Petrou et al. 2016). It is projected that these conditions will yield blooms of heavily-silicified diatom species (Deppeler and Davidson 2017) that are known to sink rapidly out of the mixed layer or, if consumed, their frustules are expected to survive the gut passages of copepods, resulting in increased carbon export (Assmy et al. 2013). However, this increase is unlikely to be two-fold that presently contributed by diatoms, and therefore not as high as the carbon export potential associated with colonial *P. antarctica.* In net, the expected floristic shift may lead to decreased carbon export at the ice shelves, in turn decreasing the carbon content of the MWDW formed at LCIS. Further investigation of the drivers of phytoplankton community composition is required to validate this notion, particularly with regards to the response of Antarctic phytoplankton to warming, as well as how changes in the surface ecosystem are transferred to and reflected in the biogeochemistry of bottom waters.

https://doi.org/10.5194/bg-2021-122
Preprint. Discussion started: 17 May 2021
© Author(s) 2021. CC BY 4.0 License.

5. Conclusions

In this study, we investigated the summertime productivity of understudied regions of the Weddell Sea, including LCIS, and the potential importance of different phytoplankton groups for biomass production, nutrient consumption, and carbon export. Our data show that mixed-layer nutrient depletion ratios were determined by the dominant phytoplankton group. The lowest Si:N and highest N:P depletion ratios were observed at LCIS (consistent with *P. antarctica* dominance), while the highest Si:N and lowest N:P depletion ratios were estimated at FIS and in the WG (consistent with diatom dominance). The variability in phytoplankton community composition appears to have been largely driven by mechanisms controlling water column stratification. *P. antarctica* are low-light specialists and proliferated at LCIS due to the deep mixed layers that occurred early in the season, while diatoms dominated at stations where the upper water column was more stratified and the mixed layer was shallow, induced by sea-ice melt. Not only does the observed relationship between phytoplankton community composition and the nutrient depletion ratios have implications for the stoichiometry of the deep-water nutrient reservoir, but it likely also has consequences for carbon export and storage.

Although the waters adjacent to LCIS were characterized by the highest NO_3^- uptake rates, the lowest f-ratios were also observed here. We attribute these low f-ratios to some degree of NH_4^+ inhibition of NO_3^- uptake, which translates to a missed opportunity for carbon export (Cochlan and Bronk 2003) and potentially, long-term storage in bottom waters, particularly since neither NO_3^- nor iron appeared to be limiting at the time of our sampling. Additional investigation is required to ascertain the persistence of NH_4^+ inhibition in the Antarctic CCSZ, particularly in regions of deep-water formation (e.g., at Filchner-Ronne Ice Shelf). Furthermore, given the prediction that the Weddell Sea's upper water column will become more stratified with climate change (Pörtner et al. 2014; Sallée et al. 2013; Stammerjohn et al. 2012), it is essential that we improve our understanding of the physical and chemical drivers of phytoplankton community composition and functioning if we are to better predict changes to carbon drawdown via the biological pump.

6. Figure and table captions

Figure 1. Maps of the Weddell Sea, Larsen C Ice Shelf (LCIS; insert a) and Fimbul Ice Shelf (FIS; insert b) showing the position of the stations where rate experiments were conducted during the Weddell Sea Expedition in January/February 2019. The symbols represent the different regions of the Weddell Sea sampled during the expedition (circle – Antarctic Peninsula (AP); cross – FIS; triangle – LCIS; plus sign – Weddell Gyre (WG)). The general cyclonic circulation of the Weddell Gyre (dashed blue arrow) is illustrated on the central map, and the dashed black arrows indicate the input of modified water masses from Filchner-Ronne Ice shelf (FRIC) and LCIS (Gordon et al. 1993; Schröder et al. 2002; Schodlok et al. 2002). The hypothesized circulation at LCIS (Nicholls et al. 2004; Hutchinson et al. 2020) is shown by the dashed blue arrow in insert (a). The 3.125 km sea-ice concentration data shown in the central panel were taken from ftp://ftp-projects.cen.uni-hamburg.de/seaice/AMSR2/3.125km and the bathymetry data (inserts a and b) were taken from ETOPO1 (NOAA National Geophysical Data Center 2009).

Figure 2. Depth profiles (0-100 m) of (a) potential density (σ_θ), (b) potential temperature, (c) absolute salinity, and (d) photosynthetically active radiation (PAR) at all stations. The inserts in panels (a), (b) and (c) show the

https://doi.org/10.5194/bg-2021-122
Preprint. Discussion started: 17 May 2021
© Author(s) 2021. CC BY 4.0 License.

profiles down to 1500 m, with the various water masses present at each station identified from their temperature and salinity ranges (WSBW – Weddell Sea Bottom Water, WSDW – Weddell Sea Deep Water, WDW – Warm Deep Water, MWDW – Modified Warm Deep Water, ISW – Ice Shelf Water, HSSW – High Salinity Shelf Water, WW – Winter Water, ASW – Antarctic Surface Water). The station positions are indicated by the different colours: red – Antarctic Peninsula, green – Larsen C Ice Shelf, blue –Weddell Gyre, light purple – early summer Fimbul Ice Shelf, and dark purple – late summer Fimbul Ice Shelf.

Figure 3. Depth profiles (0-500 m) of the concentrations of (a) NH_4^+, (b) urea-N, (c) NO_2^-, (d) NO_3^-, (e) $Si(OH)_4$ and (f) PO_4^{3-}. For all panels, the error bars represent ± 1 SD replicate samples (n = 2-3). Where applicable, the error has been propagated according to standard statistical practices.

Figure 4. Depth profiles (0-150 m) of (a) NO_3^- depletion, (b) $Si(OH)_4$ depletion and (c) PO_4^{3-} depletion at each station. Also shown are scatterplots of (d) $Si(OH)_4$ depletion versus NO_3^- depletion at each depth over the euphotic zone at all stations (grey symbols) and the theoretical euphotic zone-averaged $Si(OH)_4$ versus total N depletion (coloured symbols; see text for details) and (e) PO_4^{3-} depletion versus NO_3^- depletion at each depth over the euphotic zone at all stations (grey symbols) and the theoretical euphotic zone-averaged PO_4^{3-} versus total N depletion (coloured symbols). The dashed line in panel (d) represents the 1:1 Si:N depletion ratio, expected for iron-replete diatoms (Ragueneau et al. 2000; Hutchins and Bruland 1998; Takeda 1998; Mosseri et al. 2008), while the dotted lines represent the 1:2 Si:N ratio, indicative of enhanced activity of non-siliceous phytoplankton, and the 2:1 Si:N ratio, expected for iron-limited diatoms (Arrigo et al. 1999; Franck et al. 2000; Brzezinski et al. 2003; Green and Sambrotto 2006; Mosseri et al. 2008; Weber and Deutsch 2010; Martiny et al. 2013). The dashed line in panel (e) represents the 16:1 N:P depletion ratio (the Redfield ratio), while the dotted lines represent the 20:1 N:P ratio, expected for *P. antarctica*, and 14:1 N:P ratio, expected for iron-replete diatoms (Hutchins and Bruland 1998; Takeda 1998; Arrigo et al. 1999; Ragueneau et al. 2000; Mosseri et al. 2008).

Figure 5. Bar plots of (a, c, e) PON concentrations and (b, d,f) biomass C:N ratios measured at the 55% (a-b), 10% (c-d) and 1% light levels (e-f). The dotted black line in panels (b), (d), and (f) indicates the Redfield C:N ratio of 6.63. The error bars represent ± 1 SD of replicate samples (n = 2-6). Where applicable, the error has been propagated according to standard statistical practices.

Figure 6. Daily rates of (a, e, i) NPP, (b, f, j) ρNO_3^-, (c, g, k) ρNH_4^+ and (d, h, l) ρurea for the 55% (a-d), 10% (e-h) and 1% light level (i-l). Where there are no bars in panels (d), (h) and (l), no data are available. The error bars represent ± 1 SD of replicate samples (n = 2).

Figure 7. Depth profiles of the NO_2^- oxidation rates measured at each station (a) between the surface and 500 m, and (b) within the euphotic zone only.

Figure 8. Euphotic zone-integrated f-ratios at each station. The hashed and white bars show the difference between the $\text{f-ratio}_{(\text{excluding urea})}$ (higher value) and the $\text{f-ratio}_{(\text{including urea})}$ (lower value), with the hashed bars

https://doi.org/10.5194/bg-2021-122
Preprint. Discussion started: 17 May 2021
© Author(s) 2021. CC BY 4.0 License.

representing the stations where urea uptake was measured and the white bars where it was estimated (see text for details).

Figure 9. The (a, d) cell counts, (b, e) relative cell abundance**,** (c) log-transformed biovolume and (f) carbon biomass of all phytoplankton groups identified from the (a-c) surface flow cytometry samples and (d-f) phytoplankton net samples. Where there are no bars in panels (d), (e), and (f), no data are available. Carbon biomass estimates in panel (f) are only available for prymnesiophyte, *P. antarctica*, and the diatom species.

Figure 10. Euphotic zone-averaged rates of (a) NPP, (b) ρNO_3^- and (c) ρNH_4^+ versus Z_{eu}, and (d) NPP versus SST at each station. The symbols in panels (b) and (c) are coloured by nutrient concentration and in panel (d), by ρNO_3^- .

Figure 11. Maps of (a) SST, (b) sea surface salinity, and (c) surface oxygen concentrations, and (d) depth profiles of oxygen concentrations in the region of LCIS at the time of sampling. SST and salinity data were acquired from the underway (~7 m inflow) ferrybox, while the oxygen concentrations were measured via the oxygen sensor on the CTD profiler, calibrated against discrete seawater samples measured for dissolved oxygen by Winkler titration (Carpenter 1965; Grasshoff et al. 1983; Hutchinson et al. 2020)(Carpenter 1965; Grasshoff, Kremling, and Ehrhard 1983)(Carpenter 1965; Grasshoff, Kremling, and Ehrhard 1983)(Carpenter 1965; Grasshoff, Kremling, and Ehrhard 1983). The symbols in panel (d) are coloured by potential density (σ_θ), with the circles indicating the non-upwelling stations and the triangles the upwelling stations. The grey box in panel (d) indicates the average mixed layer depth (MLD) across the stations at LCIS. The bathymetry data in panels (a-c) were taken from ETOPO1 (NOAA National Geophysical Data Center 2009).

Figure 12. (a) NO_3^- uptake normalised to NH_4^+ uptake versus NH_4^+ concentration and b) NO_3^- depletion versus NH_4^+ concentration. The symbols in panel (a) are coloured by NH_4^+ uptake rate and in panel (b) by PON concentration. The symbol size in panel (b) represents the light level at which the samples were incubated. In panel (b), NO_3^- depletion at LCIS corresponds with the primary y-axis and NO_3^- depletion at all other stations corresponds with the secondary y-axis.

Table 1. Euphotic zone-averaged nutrient concentrations, nutrient depletions, and nutrient depletion ratios at each station occupied in the Weddell Sea in summer 2018/2019. Values shown are averages ± 1 SD ($n \geq 2$). "-" indicates no available data.

Table 2. Euphotic zone-integrated rates and averages at each station occupied in the Weddell Sea in summer 2018/2019. Values shown are averages ± 1 SD ($n \geq 2$). "-" indicates no available data and the values shown in italics (i.e., ρurea) were estimated rather than measured (see text for details).

https://doi.org/10.5194/bg-2021-122
Preprint. Discussion started: 17 May 2021
© Author(s) 2021. CC BY 4.0 License.

7. Author contributions

RF led the study and writing of the manuscript. SF contributed substantially to writing the manuscript, and designed the experiments with RF and TB. RF and JB carried out the experiments. JB, TB, SF, KS and SS assisted with sampling and data generations, and contributed to writing the manuscript.

8. Acknowledgements

We thank Captain Knowledge Bengu, Captain Freddie Ligthelm and the exceptional crew of the RV *SA Agulhas II*, as well as the Weddell Sea Expedition 2019. We also thank R. Audh, T. Henry, K. Hutchinson and H. Luyt for assistance at sea, R. Roman for help with nutrient analyses, the University of Cape Town (UCT) Marine Biogeochemistry Lab, the High Resolution Transmission Electron Microscopy Unit of the Nelson Mandela University, I. Newton and J. Luyt at the UCT Stable Light Isotope Laboratory for particle isotope measurements, K. Pecsok Ewert at the UC Davis Stable Isotope Facility for nitrate isotope measurements, and T. Reid and L. Haraguchi for assistance with flow cytometry analyses. This research was supported by the Flotilla Foundation through a grant to S.E.F. and T.B.; the South African National Antarctic Program through grants 105539, 117035 and 129232 to S.E.F.; the South African National Research Foundation through postgraduate fellowships to J.M.B., S.S. and K.A.M.S.; UCT through a Science Faculty Fellowship to R.F.F., Vice-Chancellor Doctoral Research Scholarships and Postgraduate Merit Awards to R.F.F., J.M.B. and S.S., and a Vice-Chancellor Future Leaders 2030 award to S.E.F.; and the African Academy of Sciences/Royal Society through a FLAIR Fellowship to S.E.F. The authors also acknowledge the South African Department of Science and Innovation's Biogeochemistry Research Infrastructure Platform (BIOGRIP) and Shallow Marine and Coastal Research Infrastructure (SMCRI). The data discussed in this manuscript are available in the Zenodo database and can be found at 10.5281/zenodo.4737280.

9. References

Altabet, Mark A., and Roger Francois. 2001. "Nitrogen Isotope Biogeochemistry of the Antarctic Polar Frontal Zone at 170°W." *Deep-Sea Research Part II: Topical Studies in Oceanography* 48 (19–20): 4247–73. https://doi.org/10.1016/S0967-0645(01)00088-1.

Arrigo, Kevin R., and Gert L. van Dijken. 2003. "Phytoplankton Dynamics within 37 Antarctic Coastal Polynya Systems." *Journal of Geophysical Research: Oceans* 108 (8). https://doi.org/10.1029/2002jc001739.

Arrigo, Kevin R., Gert van Dijken, and Matthew Long. 2008. "Coastal Southern Ocean: A Strong Anthropogenic CO2 Sink." *Geophysical Research Letters* 35 (21): 1–6. https://doi.org/10.1029/2008GL035624.

Arrigo, Kevin R., Giacomo R. DiTullio, Robert B. Dunbar, Dale H. Robinson, Michael VanWoert, Denise L. Worthen, and Michael P. Lizotte. 2000. "Phytoplankton Taxonomic Variability in Nutrient Utilization and Primary Production in the Ross Sea." *Journal of Geophysical Research: Oceans* 105 (C4): 8827–46. https://doi.org/10.1029/1998jc000289.

Arrigo, Kevin R., Dale H. Robinson, Denise L. Worthen, Robert B. Dunbar, Giacomo R. DiTullio, Michael VanWoert, and Michael P. Lizotte. 1999. "Phytoplankton Community Structure and the Drawdown of Nutrients and CO2 in the Southern Ocean." *Science* 283 (5400): 365–67. https://doi.org/10.1126/science.283.5400.365.

© Author(s) 2021. CC BY 4.0 License.

1097 Assmy, Philipp, Victor Smetacek, Marina Montresor, Christine Klaas, Joachim Henjes, Volker H Strass, Jesús
1098 M Arrieta, et al. 2013. “Thick-Shelled, Grazer-Protected Diatoms Decouple Ocean Carbon and Silicon
1099 Cycles in the Iron-Limited Antarctic Circumpolar Current.” *Proceedings of the National Academy of*
1100 *Sciences of the United States of America* 110 (51): 20633–38. https://doi.org/10.1073/pnas.1309345110.
1101 Baar, Hein J W De, Philip W Boyd, Kenneth H Coale, Michael R Landry, Atsushi Tsuda, Philipp Assmy,
1102 Dorothee C E Bakker, et al. 2005. “Synthesis of Iron Fertilization Experiments: From the Iron Age in the
1103 Age of Enlightenment.” *JOURNAL OF GEOPHYSICAL RESEARCH* 110: 9–16.
1104 https://doi.org/10.1029/2004JC002601.
1105 Bendschneider, Kenneth, Rex J. Robinson, John H. Margeson, Jack C. Suggs, M. Rodney Midgett, Cadmium
1106 Reduction Method, R. Dussin, et al. 2020. “A New Spectrophotometric Method for the Determination of
1107 Nitrite in Sea Water.” *Journal of Marine Research* 11 (3): 0–1.
1108 https://doi.org/10.1357/0022240963213673.
1109 Berges, John A., and Margaret R. Mulholland. 2008. *Enzymes and Nitrogen Cycling*. *Nitrogen in the Marine*
1110 *Environment*. https://doi.org/10.1016/B978-0-12-372522-6.00032-3.
1111 Böhlke, J. K., and T. B. Coplen. 1995. “Interlaboratory Comparison of Reference Materials for Nitrogenisotope-
1112 Ratio Measurements.”
1113 Böhlke, J. K., S. J. Mroczkowski, and T. B. Coplen. 2003. “Oxygen Isotopes in Nitrate: New Reference
1114 Materials for 18O: 17O: 16O Measurements and Observations on Nitrate-water Equilibration.” *Rapid*
1115 *Communications in Mass Spectrometry* 17 (16): 1835–46.
1116 Boyd, P. W., S. C. Doney, R. Strzepek, J. Dusenberry, K. Lindsay, and I. Fung. 2008. “Climate-Mediated
1117 Changes to Mixed-Layer Properties in the Southern Ocean: Assessing the Phytoplankton Response.”
1118 *Biogeosciences* 5 (3): 847–64. https://doi.org/10.5194/bg-5-847-2008.
1119 Boyd, P. W., and M. J. Ellwood. 2010. “The Biogeochemical Cycle of Iron in the Ocean.” *Nature Geoscience* 3
1120 (10): 675–82. https://doi.org/10.1038/ngeo964.
1121 Boyd, P. W., T. Jickells, C. S. Law, S. Blain, E. A. Boyle, K. O. Buesseler, K. H. Coale, et al. 2007. “Mesoscale
1122 Iron Enrichment Experiments 1993-2005: Synthesis and Future Directions.” *Science* 315 (5812): 612–17.
1123 https://doi.org/10.1126/science.1131669.
1124 Boyd, Philip W. 2004. “Ironing out Algal Issues in the Southern Ocean.” *Nature* 304 (5669): 396–97.
1125 Boyd, Philip W., and Scott C. Doney. 2002. “Modelling Regional Responses by Marine Pelagic Ecosystems to
1126 Global Climate Change.” *Geophysical Research Letters* 29 (16): 53-1-53–54.
1127 https://doi.org/10.1029/2001gl014130.
1128 BRENNECKE, and W. 1921. “Die Ozeanographischen Arbeiten Der Deutschen Antarktischen Expedition
1129 1911-12.” *Aus Dem Arciv Der Deutchen Seewarte* 39: 1–216. http://ci.nii.ac.jp/naid/10029032127/en/.
1130 Brzezinski, Mark A. 1985. “THE Si:C:N RATIO OF MARINE DIATOMS: INTERSPECIFIC VARIABILITY
1131 AND THE EFFECT OF SOME ENVIRONMENTAL VARIABLES.” *Journal of Phycology*.
1132 https://doi.org/10.1111/j.0022-3646.1985.00347.x.
1133 Brzezinski, Mark A., Mary Lynn Dickson, David M. Nelson, and Raymond Sambrotto. 2003. “Ratios of Si, C
1134 and N Uptake by Microplankton in the Southern Ocean.” *Deep-Sea Research Part II: Topical Studies in*
1135 *Oceanography* 50 (3–4): 619–33. https://doi.org/10.1016/S0967-0645(02)00587-8.
1136 Cape, Mattias R., Maria Vernet, Mati Kahru, and Gunnar Spreen. 2014. “Polynya Dynamics Drive Primary

https://doi.org/10.5194/bg-2021-122
Preprint. Discussion started: 17 May 2021
© Author(s) 2021. CC BY 4.0 License.

Production in the Larsen A and B Embayments Following Ice Shelf Collapse." *Journal of Geophysical Research: Oceans* 119 (1): 572–94. https://doi.org/10.1002/2013JC009441.

Carpenter, JH. 1965. "The Chesapeake Bay Institute Technique for the Winkler Dissolved Oxygen Method." *Limnology and Oceanography* 10 (1): 141–43.

Carvalho, Filipa, Josh Kohut, Matthew J. Oliver, and Oscar Schofield. 2017. "Defining the Ecologically Relevant Mixed-Layer Depth for Antarctica's Coastal Seas." *Geophysical Research Letters* 44 (1): 338–45. https://doi.org/10.1002/2016GL071205.

Caspel, M. van, M. Schröder, O. Huhn, and H. H. Hellmer. 2015. "Precursors of Antarctic Bottom Water Formed on the Continental Shelf off Larsen Ice Shelf." *Deep-Sea Research Part I: Oceanographic Research Papers* 99: 1–9. https://doi.org/10.1016/j.dsr.2015.01.004.

Cochlan, William P., and Deborah A. Bronk. 2003. "Effects of Ammonium on Nitrate Utilization in the Ross Sea, Antarctica: Implications for f-Ratio Estimates" 78 (3): 159–78. https://doi.org/10.1029/078ars10.

Corre, P Le, and HJ Minas. 1983. "Distributions et Évolution Des Éléments Nutritifs Dans Le Secteur Indien de l'Océan Antarctique En Wn de Période Estivale." *Oceanologica Acta* 6: 365–81.

Cota, G. F., W. O. Smith, D. M. Nelson, R. D. Muench, and L. I. Gordon. 1992. "Nutrient and Biogenic Particulate Distributions, Primary Productivity and Nitrogen Uptake in the Weddell-Scotia Sea Marginal Ice Zone during Winter." *Journal of Marine Research* 50 (1): 155–81. https://doi.org/10.1357/002224092784797764.

Delmont, Tom O., Katherine M. Hammar, Hugh W. Ducklow, Patricia L. Yager, and Anton F. Post. 2014. "Phaeocystis Antarctica Blooms Strongly Influence Bacterial Community Structures in the Amundsen Sea Polynya." *Frontiers in Microbiology* 5 (DEC): 1–13. https://doi.org/10.3389/fmicb.2014.00646.

Deppeler, Stacy L., and Andrew T. Davidson. 2017. "Southern Ocean Phytoplankton in a Changing Climate." *Frontiers in Marine Science* 4 (FEB). https://doi.org/10.3389/fmars.2017.00040.

DeVries, T. 2014. "The Oceanic Anthropogenic CO2 Sink: Storage, Air-Sea Fluxes, and Transports over the Industrial Era." *Global Biogeochemical Cycles* 28 (7): 631–47.

Diamond, D. 1994. "QuikChem Method 10-114-21-1-B: Silicate by Flow Injection Analysis."

Ditullio, G R, J M Grebmeier, K R Arrigo, and M P Lizotte. 2000. "Rapid and Early Export of Phaeocystis Antarctica Blooms in the Ross Sea , Antarctica" 404 (December 1996): 1996–99.

Dortch, Q. 1990. "The Interaction between Ammonium and Nitrate Uptake in Phytoplankton." *Marine Ecology Progress Series* 61 (1): 183–201. https://doi.org/10.3354/meps061183.

Dubelaar, George B.J., and R. R. Jonker. 2000. "Flow Cytometry as a Tool for the Study of Phytoplankton." *Scientia Marina* 64 (2): 135–56. https://doi.org/10.3989/scimar.2000.64n2135.

Dugdale, R. C., and J. J. Goering. 1967. "Uptake of New and Regenerated Forms of Nitrogen in Primary Productivity." *Limnology and Oceanography* 12 (2): 196–206. https://doi.org/10.4319/lo.1967.12.2.0196.

Dugdale, R C, and F P Wilkerson. 1986. "The Use of 15N to Measure Nitrogen Uptake in Eutrophic Experimental Considerations1 T2" 3 (July).

Eicken, Hajo. 1993. "The Role of Sea Ice in Structuring Antarctic Ecosystems." In *Weddell Sea Ecology*, edited by Gotthilf Hempel, 3–13. Berlin, Heidelberg: Springer Berlin Heidelberg.

El-Sayed, S. 1984. "Productivity of the Antarctic Waters — A Reappraisal." In *Marine Phytoplankton and Productivity. Lecture Notes on Coastal and Estuarine Studies.*, edited by Holm-Hansen O., Bolis L., and

© Author(s) 2021. CC BY 4.0 License.

1177 Gilles R., 8th ed., 19–34. Springer Berlin Heidelberg.
1178 El-Sayed, Sayed Z., and Satoru Taguchi. 1981. "Primary Production and Standing Crop of Phytoplankton along
1179 the Ice-Edge in the Weddell Sea." *Deep Sea Research Part A, Oceanographic Research Papers* 28 (9):
1180 1017–32. https://doi.org/10.1016/0198-0149(81)90015-7.
1181 Eppley, R. W., Peterson, B. 1979. "Particulate Organic Matter Flux and Planktonic New Production in the Deep
1182 Ocean." *Nature* 282: 677–80.
1183 Fahrbach, E., G. Rohardt, N. Scheele, M. Schroder, V. Strass, and A. Wisotzki. 1995. "Formation and Discharge
1184 of Deep and Bottom Water in the Northwestern Weddell Sea." *Journal of Marine Research* 53 (4): 515–
1185 38. https://doi.org/10.1357/0022240953213089.
1186 Fahrbach, E., G. Rohardt, M. Schröder, and V. Strass. 1994. "Transport and Structure of the Weddell Gyre."
1187 *Annales Geophysicae* 12 (9): 840–55. https://doi.org/10.1007/s00585-994-0840-7.
1188 Fawcett, S. E., and B. B. Ward. 2011. "Phytoplankton Succession and Nitrogen Utilization during the
1189 Development of an Upwelling Bloom." *Marine Ecology Progress Series* 428: 13–31.
1190 https://doi.org/10.3354/meps09070.
1191 Ferreira, Afonso, Raul R. Costa, Tiago S. Dotto, Rodrigo Kerr, Virginia M. Tavano, Ana C. Brito, Vanda
1192 Brotas, Eduardo R. Secchi, and Carlos R.B. Mendes. 2020. "Changes in Phytoplankton Communities
1193 Along the Northern Antarctic Peninsula: Causes, Impacts and Research Priorities." *Frontiers in Marine*
1194 *Science* 7 (October). https://doi.org/10.3389/fmars.2020.576254.
1195 Franck, Valerie M., Mark A. Brzezinski, Kenneth H. Coale, and David M. Nelson. 2000. "Iron and Silicic Acid
1196 Concentrations Regulate Si Uptake North and South of the Polar Frontal Zone in the Pacific Sector of the
1197 Southern Ocean." *Deep-Sea Research Part II: Topical Studies in Oceanography* 47 (15–16): 3315–38.
1198 https://doi.org/10.1016/S0967-0645(00)00070-9.
1199 Fripiat, F., D. M. Sigman, S. E. Fawcett, P. A. Rafter, M. A. Weigand, and J.-L. Tison. 2014. "New Insights into
1200 Sea Ice Nitrogen Biogeochemical Dynamics from the Nitrogen Isotopes." *Global Biogeochemical Cycles*
1201 28 (2): 115–30. https://doi.org/10.1002/2013GB004729.
1202 Frölicher, T. L., J. L. Sarmiento, D. J. Paynter, J. P. Dunne, J. P. Krasting, and M Winton. 2015. "Dominance of
1203 the Southern Ocean in Anthropogenic Carbon and Heat Uptake in CMIP5 Models." *Journal of Climate* 28
1204 (2): 862–86.
1205 Garcia, Nathan S., Julie Sexton, Tracey Riggins, Jeff Brown, Michael W. Lomas, and Adam C. Martiny. 2018.
1206 "High Variability in Cellular Stoichiometry of Carbon, Nitrogen, and Phosphorus within Classes of
1207 Marine Eukaryotic Phytoplankton under Sufficient Nutrient Conditions." *Frontiers in Microbiology* 9
1208 (MAR): 1–10. https://doi.org/10.3389/fmicb.2018.00543.
1209 Gill, A. E. 1973. "Circulation and Bottom Water Production in the Weddell Sea." *Deep-Sea Research and*
1210 *Oceanographic Abstracts* 20 (2): 111–40. https://doi.org/10.1016/0011-7471(73)90048-X.
1211 Gleitz, Markus, Michiel Rutgers Michiel, David N. Thomas, Gerhard S. Dieckmann, and Frank J. Millero. 1995.
1212 "Comparison of Summer and Winter Inorganic Carbon, Oxygen and Nutrient Concentrations in Antarctic
1213 Sea Ice Brine." *Marine Chemistry* 51 (2): 81–91. https://doi.org/10.1016/0304-4203(95)00053-T.
1214 Glibert, Patricia M., Frances P. Wilkerson, Richard C. Dugdale, John A. Raven, Christopher L. Dupont, Peter R.
1215 Leavitt, Alexander E. Parker, Joann M. Burkholder, and Todd M. Kana. 2016. "Pluses and Minuses of
1216 Ammonium and Nitrate Uptake and Assimilation by Phytoplankton and Implications for Productivity and

https://doi.org/10.5194/bg-2021-122
Preprint. Discussion started: 17 May 2021
© Author(s) 2021. CC BY 4.0 License.

1217 Community Composition, with Emphasis on Nitrogen-Enriched Conditions." *Limnology and*
1218 *Oceanography* 61 (1): 165–97. https://doi.org/10.1002/lno.10203.
1219 Goeyens, L. 1991. "Ammonium Regeneration in the Scotia-Weddell Confluence Area during Spring 1988."
1220 *Marine Ecology Progress Series* 78 (3): 241–52. https://doi.org/10.3354/meps078241.
1221 Goeyens, L., P. Tréguer, M. E.M. Baumann, W. Baeyens, and F. Dehairs. 1995. "The Leading Role of
1222 Ammonium in the Nitrogen Uptake Regime of Southern Ocean Marginal Ice Zones." *Journal of Marine*
1223 *Systems* 6 (4): 345–61. https://doi.org/10.1016/0924-7963(94)00033-8.
1224 Goffart, A., G. Catalano, and J. H. Hecq. 2000. "Factors Controlling the Distribution of Diatoms and
1225 Phaeocystis in the Ross Sea." *Journal of Marine Systems* 27 (1–3): 161–75.
1226 https://doi.org/10.1016/S0924-7963(00)00065-8.
1227 Gonfiantini, R. 1984. "Stable Isotope Reference Samples for Geochemical and Hydrological Investigations."
1228 *Report of Advisory Group, Vienna*.
1229 Gordon, A. L., Huber, B. A., Hellmer, H. H., & Ffield, A. 1993. "Deep and Bottom Water of the Weddell Sea's
1230 Western Rim." *Science* 265 (5130): 95–97.
1231 Granger, Julie, and Daniel M. Sigman. 2009. "Removal of Nitrite with Sulfamic Acid for Nitrate N and O
1232 Isotope Analysis with the Denitrifier Method." *Rapid Communications in Mass Spectrometry* 23 (23):
1233 3753–62. https://doi.org/10.1002/rcm.4307.
1234 Grasshoff, K. 1976. *Methods of Seawater Analysis*. Weinheim and New York: Verlag Chemie.
1235 Grasshoff, K, K Kremling, and M Ehrhard. 1983. *Methods of Seawater Analysis*. Florida: Verlag Chemia.
1236 Green, Sara E., and Raymond N. Sambrotto. 2006. "Plankton Community Structure and Export of C, N, P and
1237 Si in the Antarctic Circumpolar Current." *Deep-Sea Research Part II: Topical Studies in Oceanography*
1238 53 (5–7): 620–43. https://doi.org/10.1016/j.dsr2.2006.01.022.
1239 Gruber, N., D. Clement, B. R. Carter, R. A. Feely, S. Van Heuven, and M. Hoppema. 2019. "The Oceanic Sink
1240 for Anthropogenic CO2 from 1994 to 2007." *Science* 363: 1193–99.
1241 Guerrero, Maria A., and Ronald D. Jones. 1996. "Photoinhibition of Marine Nitrifying Bacteria. II. Dark
1242 Recovery after Monochromatic or Polychromatic Irradiation." *Marine Ecology Progress Series* 141: 193–
1243 98. https://doi.org/10.3354/meps141193.
1244 Hansen, B, Bjornsen PK, Hansen PJ. 1994. "The Size Ratio between Planktonic Predators and Their Prey."
1245 *Limnology and Oceanography* 39 (2): 395–403.
1246 Henley, Sian F., Robyn E. Tuerena, Amber L. Annett, Anthony E. Fallick, Michael P. Meredith, Hugh J.
1247 Venables, Andrew Clarke, and Raja S. Ganeshram. 2017. "Macronutrient Supply, Uptake and Recycling
1248 in the Coastal Ocean of the West Antarctic Peninsula." *Deep-Sea Research Part II: Topical Studies in*
1249 *Oceanography* 139 (xxxx): 58–76. https://doi.org/10.1016/j.dsr2.2016.10.003.
1250 Holmes, R M, A Aminot, R Kerouel, B A Hooker, and B J Peterson. 1999. "A Simple and Precise Method for
1251 Measuring Ammonium in Marine and Freshwater Ecosystems." *Canadian Journal of Fisheries and*
1252 *Aquatic Sciences*. https://doi.org/10.1139/cjfas-56-10-1801.
1253 Hoppema, M., and L. Goeyens. 1999. "Redfield Behavior of Carbon, Nitrogen, and Phosphorus Depletions in
1254 Antarctic Surface Water." *Limnology and Oceanography* 44 (1): 220–24.
1255 https://doi.org/10.4319/lo.1999.44.1.0220.
1256 Hoppema, M, R Middag, H de Baar, E Fahrbach, E van Weerlee, and H Thomas. 2007. "Whole Season Net

https://doi.org/10.5194/bg-2021-122
Preprint. Discussion started: 17 May 2021
© Author(s) 2021. CC BY 4.0 License.

1257 Community Production in the Weddell Sea." *Polar Biology* 31: 101–11.
1258 Hoppema, Mario. 2004. "Weddell Sea Is a Globally Significant Contributor to Deep-Sea Sequestration of
1259 Natural Carbon Dioxide." *Deep-Sea Research Part I: Oceanographic Research Papers* 51 (9): 1169–77.
1260 https://doi.org/10.1016/j.dsr.2004.02.011.
1261 Hoppema, Mario, Karel Bakker, Steven MAC van Heuven, Jan C van Ooijen, and Hein JW de Baar. 2015.
1262 "Distributions, Trends and Inter-Annual Variability of Nutrients along a Repeat Section through the
1263 Weddell Sea (1996-2011)." https://doi.org/10.1016/j.marchem.2015.08.007.
1264 Hoppema, Mario, Leo Goeyens, and Eberhard Fahrbach. 2000. "Intense Nutrient Removal in the Remote Area
1265 off Larsen Ice Shelf (Weddell Sea)." *Polar Biology* 23 (2): 85–94.
1266 https://doi.org/10.1007/s003000050012.
1267 Hoppema, Mario, Michel H.C. Stoll, and Hein J.W. De Baar. 2000. "Co2 in the Weddell Gyre and Antarctic
1268 Circumpolar Current: Austral Autumn and Early Winter." *Marine Chemistry* 72 (2–4): 203–20.
1269 https://doi.org/10.1016/S0304-4203(00)00082-7.
1270 Horrigan, Sarah G. 1981. "Primary Production under the Ross Ice Shelf, Antarctica." *Limnology and*
1271 *Oceanography* 26 (2): 378–82. https://doi.org/10.4319/lo.1981.26.2.0378.
1272 Huhn, Oliver, Hartmut H. Hellmer, Monika Rhein, Christian Rodehacke, Wolfgang Roether, Michael P.
1273 Schodlok, and Michael Schröder. 2008. "Evidence of Deep- and Bottom-Water Formation in the Western
1274 Weddell Sea." *Deep-Sea Research Part II: Topical Studies in Oceanography* 55 (8–9): 1098–1116.
1275 https://doi.org/10.1016/j.dsr2.2007.12.015.
1276 Hutchins, David A., and K. W. Bruland. 1998. "Iron-Limited Growth and Si:N Ratios in a Costal Upwelling
1277 Regime." *Nature* 393 (June): 561–64.
1278 Hutchinson, Katherine, Julie Deshayes, Jean Baptiste Sallee, Julian A. Dowdeswell, Casimir de Lavergne,
1279 Isabelle Ansorge, Hermann Luyt, Tahlia Henry, and Sarah E. Fawcett. 2020. "Water Mass Characteristics
1280 and Distribution Adjacent to Larsen C Ice Shelf, Antarctica." *Journal of Geophysical Research: Oceans*
1281 125 (4): 0–2. https://doi.org/10.1029/2019JC015855.
1282 Ito, T, M Woloszyn, and & M Mazloff. 2010. "Anthropogenic Carbon Dioxide Transport in the Southern Ocean
1283 Driven by Ekman Flow" 463 (7). https://doi.org/10.1038/nature08687.
1284 Jacobs, S. S. 1986. "The Antarctic Slope Front." *Antarct. JUS* 21 (5): 123–24.
1285 Jacobs, Stanley S. 1991. "On the Nature and Significance of the Antarctic Slope Front." *Marine Chemistry* 35
1286 (1–4): 9–24. https://doi.org/10.1016/S0304-4203(09)90005-6.
1287 Jacques, G. 1991. "Is the Concept of New Production—Regenerated Production Valid for the Southern Ocean?"
1288 *Marine Chemistry* 35 (1–4): 273–86. https://doi.org/10.1016/S0304-4203(09)90022-6.
1289 Jennings, Joe C., Louis I. Gordon, and David M. Nelson. 1984. "Nutrient Depletion Indicates High Primary
1290 Productivity in the Weddell Sea." *Nature* 309 (5963): 51–54. https://doi.org/10.1038/309051a0.
1291 Jong, Jeroen De, Véronique Schoemann, Delphine Lannuzel, Peter Croot, Hein De Baar, and Jean Louis Tison.
1292 2012. "Natural Iron Fertilization of the Atlantic Sector of the Southern Ocean by Continental Shelf
1293 Sources of the Antarctic Peninsula." *Journal of Geophysical Research: Biogeosciences* 117 (1).
1294 https://doi.org/10.1029/2011JG001679.
1295 Juel Hansen, Per, Peter Koefoed Bj, and Benni Winding Hansen. 1997. "Zooplankton Grazing and Growth:
1296 Scaling within the 2-2,000-~III Body Size Range." Vol. 42.

https://doi.org/10.5194/bg-2021-122
Preprint. Discussion started: 17 May 2021
© Author(s) 2021. CC BY 4.0 License.

1297 Kana, Todd M., and Patricia M. Glibert. 1987. "Effect of Irradiances up to 2000 ME M-2 s-1 on Marine
1298 Synechococcus WH7803-I. Growth, Pigmentation, and Cell Composition." *Deep Sea Research Part A,*
1299 *Oceanographic Research Papers* 34 (4): 479–95. https://doi.org/10.1016/0198-0149(87)90001-X.
1300 Kaprelyants, A. S., and D. B. Kell. 1993. "Dormancy in Stationary-Phase Cultures of Micrococcus Luteus: Flow
1301 Cytometric Analysis of Starvation and Resuscitation." *1Applied and Environmental Microbiology* 59 (10):
1302 3187–96.
1303 Keffer, T., and G. Holloway. 1988. "Estimating Southern Ocean Eddy Flux of Heat and Salt from Satellite
1304 Altimetry." *Nature* 332 (6165): 624–26. https://doi.org/10.1038/332624a0.
1305 Keller, D.P., L. Kriest, W. Koeve, and A. Oschlies. 2016. "Southern Ocean Biological Impacts on Global Ocean
1306 Oxygen." *Geophysical Research Letters* 43: 6469–77.
1307 Kerr, Rodrigo, Mauricio M. Mata, Carlos Rafael B. Mendes, and Eduardo R. Secchi. 2018. "Northern Antarctic
1308 Peninsula: A Marine Climate Hotspot of Rapid Changes on Ecosystems and Ocean Dynamics." *Deep-Sea*
1309 *Research Part II: Topical Studies in Oceanography* 149 (March): 4–9.
1310 https://doi.org/10.1016/j.dsr2.2018.05.006.
1311 Klunder, M. B., P. Laan, H. J. W. De Baar, R. Middag, I. Neven, and J. Van Ooijen. 2014. "Dissolved Fe across
1312 the Weddell Sea and Drake Passage: Impact of DFe on Nutrient Uptake." *Biogeosciences* 11 (3): 651–69.
1313 https://doi.org/10.5194/bg-11-651-2014.
1314 Klunder, M. B., P. Laan, R. Middag, H. J.W. De Baar, and J. C. van Ooijen. 2011. "Dissolved Iron in the
1315 Southern Ocean (Atlantic Sector)." *Deep-Sea Research Part II: Topical Studies in Oceanography* 58 (25–
1316 26): 2678–94. https://doi.org/10.1016/j.dsr2.2010.10.042.
1317 Koike, I, O Holm-Hansen, and DC Biggs. 1986. "Inorganic Nitrogen Metabolism by Antarctic Phytoplankton
1318 with Special Reference to Ammonium Cycling." *Marine Ecology Progress Series* 30 (2–3): 105–16.
1319 https://doi.org/10.3354/meps030105.
1320 Lannuzel, Delphine, Véronique Schoemann, Jeroen de Jong, Lei Chou, Bruno Delille, Sylvie Becquevort, and
1321 Jean Louis Tison. 2008. "Iron Study during a Time Series in the Western Weddell Pack Ice." *Marine*
1322 *Chemistry* 108 (1–2): 85–95. https://doi.org/10.1016/j.marchem.2007.10.006.
1323 Leblanc, K, Armand L, Assmy P, Beker B, Bode A, Breton E, Cornet V, et al. 2012. "A Global Diatom
1324 Database – Abundance, Biovolume and Biomass in the World Ocean." *Earth System Science Data* 4:
1325 419–165.
1326 Llort, Joan, Marina Lévy, Jean-Baptiste Sallée, and Alessandro Tagliabue. n.d. "Onset, Intensification, and
1327 Decline of Phytoplankton Blooms in the Southern Ocean." *Journal of Marine Science* 72: 1971–84.
1328 https://doi.org/10.1093/icesjms/fsv053.
1329 Locarnini, R. A., T. Whitworth, and W. D. Nowlin. 1993. "The Importance of the Scotia Sea on the Outflow of
1330 Weddell Sea Deep Water." *Journal of Marine Research* 51 (1): 135–53.
1331 https://doi.org/10.1357/0022240933223846.
1332 Lomas, M. W., and P. M. Glibert. 1999. "Interactions between NH4/+ and NO3/- Uptake and Assimilation:
1333 Comparison of Diatoms and Dinoflagellates at Several Growth Temperatures." *Marine Biology* 133 (3):
1334 541–51. https://doi.org/10.1007/s002270050494.
1335 Malone, T. 1980. "Size-Fractionated Primary Productivity of Marine Phytoplankton." In *Environmental Science*
1336 *Research*, 301–19.

https://doi.org/10.5194/bg-2021-122
Preprint. Discussion started: 17 May 2021
© Author(s) 2021. CC BY 4.0 License.

1337 Marchetti, A., and N. Cassar. 2009. “Diatom Elemental and Morphological Changes in Response to Iron
1338 Limitation: A Brief Review with Potential Paleoceanographic Applications.” *Geobiology* 7 (4): 419–31.
1339 https://doi.org/10.1111/j.1472-4669.2009.00207.x.
1340 Marchetti, Adrian, and Maria T Maldonado. 2016. *The Physiology of Microalgae*. *The Physiology of*
1341 *Microalgae*. https://doi.org/10.1007/978-3-319-24945-2.
1342 Martin, John H., R. Michael Gordon, and Steve E. Fitzwater. 1991. “Iron Limitation.” *Limnology and*
1343 *Oceanography* 36 (8): 1793–1802.
1344 http://doi.wiley.com/10.4319/lo.1991.36.8.1793%0Ahttp://onlinelibrary.wiley.com/store/10.4319/lo.1991.
1345 36.8.1793/asset/lno19913681793.pdf?v=1&t=j6qdk51h&s=456915f948d9c4ef90e914c1583d2396c4bfe2b
1346 6.
1347 Martínez-García, Alfredo, Daniel M Sigman, Haojia Ren, Robert F Anderson, Marietta Straub, David A Hodell,
1348 Samuel L Jaccard, Timothy I Eglinton, and Gerald H Haug. 2014. “Iron Fertilization of the Subantarctic
1349 Ocean During the Last Ice Age.” www.sciencemag.org.
1350 Martiny, Adam C, Chau T A Pham, Francois W Primeau, Jasper A Vrugt, J Keith Moore, Simon A Levin, and
1351 Michael W Lomas. 2013. “Strong Latitudinal Patterns in the Elemental Ratios of Marine Plankton and
1352 Organic Matter.” *Nature Geoscience*. https://doi.org/10.1038/NGEO1757.
1353 Mathot, Sylvie, Walker O. Smith, Craig A. Carlson, David L. Garrison, Marcia M. Gowing, and Chrystal L.
1354 Vickers. 2000. “Carbon Partitioning within Phaeocystis Antarctica (Prymnesiophyceae) Colonies in the
1355 Ross Sea, Antarctica.” *Journal of Phycology* 36 (6): 1049–56. https://doi.org/10.1046/j.1529-
1356 8817.2000.99078.x.
1357 McIlvin, Matthew R., and Karen L. Casciotti. 2011. “Technical Updates to the Bacterial Method for Nitrate
1358 Isotopic Analyses.” *Analytical Chemistry* 83 (5): 1850–56. https://doi.org/10.1021/ac1028984.
1359 Mdutyana, Mhlangabezi, Sandy J. Thomalla, Raissa Philibert, Bess B. Ward, and Sarah E. Fawcett. 2020. “The
1360 Seasonal Cycle of Nitrogen Uptake and Nitrification in the Atlantic Sector of the Southern Ocean.”
1361 *Global Biogeochemical Cycles* 34 (7): 1–29. https://doi.org/10.1029/2019GB006363.
1362 Merbt, Stephanie N, David A Stahl, Emilio O Casamayor, Eugè Nia Martí, Graeme W Nicol, and James I
1363 Prosser. n.d. “Differential Photoinhibition of Bacterial and Archaeal Ammonia Oxidation.”
1364 https://doi.org/10.1111/j.1574-6968.2011.02457.x.
1365 Mosby, H. 1934. “The Waters of the Atlantic Anarctic Ocean.” *Science Research Norweigan Antarctic*
1366 *Expedition 1927-1928* 11: 1–311.
1367 Mosseri, Julie, Bernard Quéguiner, Leanne Armand, and Véronique Cornet-Barthaux. 2008. “Impact of Iron on
1368 Silicon Utilization by Diatoms in the Southern Ocean: A Case Study of Si/N Cycle Decoupling in a
1369 Naturally Iron-Enriched Area.” *Deep-Sea Research Part II: Topical Studies in Oceanography* 55 (5–7):
1370 801–19. https://doi.org/10.1016/j.dsr2.2007.12.003.
1371 Muench, R. D., and A. L. Gordon. 1995. “Circulation and Transport of Water along the Western Weddell Sea
1372 Margin.” *Journal of Geophysical Research* 100 (C9): 18503–15. https://doi.org/10.1029/95jc00965.
1373 Myung Gil, Park, Tang Sung Ryull, Kang Sung-Ho, Chung Kyung Ho, and Shim Jae Hyung. 1999.
1374 “Phytoplankton Biomass and Primary Production in the Marginal Ice Zone of the Northwestern Weddell
1375 Sea during Austral Summer.” *Polar Biology* 21: 251–61.
1376 Nelson, M, O Smith, I Gordon, and A Huber. 1987. “Nutrient” 92: 7181–90.

https://doi.org/10.5194/bg-2021-122
Preprint. Discussion started: 17 May 2021
© Author(s) 2021. CC BY 4.0 License.

1377 Nicholls, K. W., C. J. Pudsey, and P. Morris. 2004. “Summertime Water Masses off the Northern Larsen C Ice
1378 Shelf, Antarctica.” *Geophysical Research Letters* 31 (9): 2–5. https://doi.org/10.1029/2004GL019924.
1379 Nicholls, Keith W., Svein Østerhus, Keith Makinson, Tor Gammelsrød, and Eberhard Fahrbach. 2009. “Ice-
1380 Ocean Processes over the Continental Shelf of the Southern Weddell Sea, Antarctica: A Review.” *Reviews*
1381 *of Geophysics* 47 (3): 1–23. https://doi.org/10.1029/2007RG000250.
1382 Nissen, Cara, and Meike Vogt. 2020. “Factors Controlling the Competition between
1383 <I>Phaeocystis</I> and Diatoms in the Southern Ocean.” *Biogeosciences Discussions*, no.
1384 January: 1–39. https://doi.org/10.5194/bg-2019-488.
1385 Olson, Robert J. 1981. “DIFFERENTIAL PHOTOINHIBITION OF MARINE NITRIFYING BACTERIA: A
1386 POSSIBLE MECHANISM FOR THE FORMATION OF THE PRIMARY NITRITE MAXIMUM.”
1387 *Journal of Marine Research* 39 (2): 227–38.
1388 Orsi, Alejandro H., Worth D. Nowlin, and Thomas Whitworth. 1993. “On the Circulation and Stratification of
1389 the Weddell Gyre.” *Deep-Sea Research Part I* 40 (1): 169–203. https://doi.org/10.1016/0967-
1390 0637(93)90060-G.
1391 Orsi, Alejandro H., Thomas Whitworth, and Worth D. Nowlin. 1995. “On the Meridional Extent and Fronts of
1392 the Antarctic Circumpolar Current.” *Deep-Sea Research Part I* 42 (5): 641–73.
1393 https://doi.org/10.1016/0967-0637(95)00021-W.
1394 Parsons, T.R., Y. Maita, and C.M. Lalli. 1984. *A Manual of Chemical and Biological Methods for Seawater*
1395 *Analysis*.
1396 Paulsen, M. L., K. Riisgaard, T. F. Thingstad, M. S. John, and T. G. Nielsen. 2015. “Winter-Spring Transition in
1397 the Subarctic Atlantic: Microbial Response to Deep Mixing and Pre-Bloom Production.” *Aquatic*
1398 *Microbial Ecology2* 76 (1): 49–49.
1399 Peng, X., C. A. Fuchsman, A. Jayakumar, S. Oleynik, W. Martens-Habbena, A. H. Devol, and B. B. Ward.
1400 2015. “Ammonia and Nitrite Oxidation in the Eastern Tropical North Pacific.” *Global Biogeochemical*
1401 *Cycles2* 29: 2034–49.
1402 Peng, Xuefeng, Sarah E Fawcett, Nicolas Van Oostende, Martin J Wolf, Dario Marconi, Daniel M Sigman, and
1403 Bess B Ward. 2018. “Nitrogen Uptake and Nitrification in the Subarctic North Atlantic Ocean.”
1404 https://doi.org/10.1002/lno.10784.
1405 Petrou, Katherina, Sven A. Kranz, Scarlett Trimborn, Christel S. Hassler, Sonia Blanco Ameijeiras, Olivia
1406 Sackett, Peter J. Ralph, and Andrew T. Davidson. 2016. “Southern Ocean Phytoplankton Physiology in a
1407 Changing Climate.” *Journal of Plant Physiology* 203: 135–50.
1408 https://doi.org/10.1016/j.jplph.2016.05.004.
1409 Pörtner, Hans Otto, D.M. Karl, P. W. Boyd, W.W. Cheung, S E Lluch-Cota, Y. Nojiri, and Al. Et. 2014. “Ocean
1410 Systems.” In *Impacts, Adaptation, and Vulnerability. Part A: Global and Sectoral Aspects. Contribution*
1411 *of Working Group II to the Fifth Assessment Report of the Intergovernmental Panel on Climate Change*,
1412 edited by C.B. Field and Al. Et, 411–84. Cambridge University Press.
1413 Priddle, J., I. L. Boyd, M. J. Whitehouse, E. J. Murphy, and J. P. Croxall. 1998. “Estimates of Southern Ocean
1414 Primary Production - Constraints from Predator Carbon Demand and Nutrient Drawdown.” In *Journal of*
1415 *Marine Systems*, 17:275–88. Elsevier. https://doi.org/10.1016/S0924-7963(98)00043-8.
1416 Probyn, T. A., and S. J. Painting. 1985. “Nitrogen Uptake by Size-fractionated Phytoplankton Populations in

© Author(s) 2021. CC BY 4.0 License.

1417 Antarctic Surface Waters." *Limnology and Oceanography* 30 (6): 1327–32.
1418 https://doi.org/10.4319/lo.1985.30.6.1327.
1419 Qin, Wei, Shady A. Amin, Willm Martens-Habbena, Christopher B. Walker, Hidetoshi Urakawa, Allan H.
1420 Devol, Anitra E. Ingalls, James W. Moffett, E. Virginia Armbrust, and David A. Stahl. 2014. "Marine
1421 Ammonia-Oxidizing Archaeal Isolates Display Obligate Mixotrophy and Wide Ecotypic Variation."
1422 *Proceedings of the National Academy of Sciences* 111 (34): 12504–9.
1423 https://doi.org/10.1073/PNAS.1324115111.
1424 Ragueneau, O., P. Tréguer, A. Leynaert, R. F. Anderson, M. A. Brzezinski, D. J. DeMaster, R. C. Dugdale, et al.
1425 2000. "A Review of the Si Cycle in the Modern Ocean: Recent Progress and Missing Gaps in the
1426 Application of Biogenic Opal as a Paleoproductivity Proxy." *Global and Planetary Change* 26 (4): 317–
1427 65. https://doi.org/10.1016/S0921-8181(00)00052-7.
1428 Revilla, Marta, Jeffrey Alexander, and Patricia M. Glibert. 2005. "Urea Analysis in Coastal Waters: Comparison
1429 of Enzymatic and Direct Methods." *Limnology and Oceanography: Methods* 3 (7): 290–99.
1430 https://doi.org/10.4319/lom.2005.3.290.
1431 Rönner, U., F. Sörensson, and O. Holm-Hansen. 1983. "Nitrogen Assimilation by Phytoplankton in the Scotia
1432 Sea." *Polar Biology* 2 (3): 137–47. https://doi.org/10.1007/BF00448963.
1433 Rubin, SI, Takahashi T, Chipman DW, and Goddard JG. 1998. "Primary Productivity and Nutrient Utilization
1434 Ratios in the Pacific Sector of the Southern Ocean Based on Seasonal Changes in Seawater Chemistry."
1435 *Deep Sea Research Part I: Oceanographic Research Papers* 45: 1211–34.
1436 Sallée, J. B., E. Shuckburgh, N. Bruneau, A. J. Meijers, T. J. Bracegirdle, and Z. Wang. 2013. "Assessment of
1437 Southern Ocean Mixed-layer Depths in CMIP5 Models: Historical Bias and Forcing Response." *Journal*
1438 *of Geophysical Research : Oceans* 118: 1845–62.
1439 Santoro, A. E., C. M. Sakamoto, J. M. Smith, J. N. Plant, A. L. Gehman, A. Z. Worden, K. S. Johnson, C. A.
1440 Francis, and K. L. Casciotti. 2013. "Measurements of Nitrite Production in and around the Primary Nitrite
1441 Maximum in the Central California Current." *Biogeosciences* 10 (11): 7395–7410.
1442 https://doi.org/10.5194/bg-10-7395-2013.
1443 Sarmiento, J., Toggweiler, J. 1984. "A New Model for the Role of the Oceans in Determining Atmospheric P
1444 CO2." *Nature* 308: 621–24. https://doi.org/https://doi.org/10.1038/308621a0.
1445 Sarmiento, J L, N Gruber, M A Brzezinski, and J P Dunne. 2004. "High-Latitude Controls of Thermocline
1446 Nutrients and Low Latitude Biological Productivity." *Nature* 427 (6969): 56–60.
1447 https://doi.org/10.1038/nature10605.
1448 Saxberg, Bo E.H., and B. R. Kowalski. 1979. "Generalized Standard Addition Method." *Analytical Chemistry*
1449 51 (7): 1031–38. https://doi.org/10.1021/ac50043a059.
1450 Scharek, Renate, Victor Smetacek, Eberhard Fahrbach, Louis I. Gordon, Gerd Rohardt, and Stanley Moore.
1451 1994. "The Transition from Winter to Early Spring in the Eastern Weddell Sea, Antarctica: Plankton
1452 Biomass and Composition in Relation to Hydrography and Nutrients." *Deep-Sea Research Part I* 41 (8):
1453 1231–50. https://doi.org/10.1016/0967-0637(94)90042-6.
1454 Schodlok, M. P., Hellmer, H. H.,&Beckmann, A. 2002. "On the Transport, Variability and Origin of
1455 Densewatermasses Crossing the South Scotia Ridge.E." *Deep Sea Research II: Tropical Studies in*
1456 *Oceanography* 49 (21): 4807–25.

https://doi.org/10.5194/bg-2021-122
Preprint. Discussion started: 17 May 2021
© Author(s) 2021. CC BY 4.0 License.

1457 Schoemann, Véronique, Sylvie Becquevort, Jacqueline Stefels, Véronique Rousseau, and Christiane Lancelot.
1458 2005. "Phaeocystis Blooms in the Global Ocean and Their Controlling Mechanisms: A Review." *Journal*
1459 *of Sea Research* 53 (1-2 SPEC. ISS.): 43–66. https://doi.org/10.1016/j.seares.2004.01.008.
1460 Schofield, Oscar, Travis Miles, Anne Carlijn Alderkamp, Sang Hoon Lee, Christina Haskins, Emily Rogalsky,
1461 Rachel Sipler, Robert M. Sherrell, and Patricia L. Yager. 2015. "In Situ Phytoplankton Distributions in the
1462 Amundsen Sea Polynya Measured by Autonomous Gliders." *Elementa* 3: 1–17.
1463 https://doi.org/10.12952/journal.elementa.000073.
1464 Schröder, M., H. H. Hellmer, and J. M. Absy. 2002. "On the Near-Bottom Variability in the Northwestern
1465 Weddell Sea." *Deep-Sea Research Part II: Topical Studies in Oceanography* 49 (21): 4767–90.
1466 https://doi.org/10.1016/S0967-0645(02)00158-3.
1467 Sedwick, Peter N., Giacomo R. Di Tullio, and Denis J. Mackey. 2000. "Iron and Manganese in the Ross Sea,
1468 Seasonal Iron Limitation in Antarctic." *Journal of Geophysical Research: Oceans* 105 (C5): 11321–36.
1469 https://doi.org/10.1029/2000JC000256.
1470 Semeneh, M., F. Dehairs, M. Elskens, M. E.M. Baumann, E. E. Kopczynska, C. Lancelot, and L. Goeyens.
1471 1998. "Nitrogen Uptake Regime and Phytoplankton Community Structure in the Atlantic and Indian
1472 Sectors of the Southern Ocean." *Journal of Marine Systems* 17 (1–4): 159–77.
1473 https://doi.org/10.1016/S0924-7963(98)00036-0.
1474 Sigman, D. M., K. L. Casciotti, M. Andreani, C. Barford, M. Galanter, and J. K. Böhlke. 2001. "A Bacterial
1475 Method for the Nitrogen Isotopic Analysis of Nitrate in Seawater and Freshwater." *Analytical Chemistry*
1476 73 (17): 4145–53. https://doi.org/10.1021/ac010088e.
1477 Sigman, Daniel M, and Edward A Boyle[2]. 2000. "Glacial/Interglacial Variations in Atmospheric Carbon
1478 Dioxide." *NATURE*. Vol. 407. www.nature.com.
1479 Sigman, Daniel M, Mathis P Hain, and Gerald H Haug. 2010. "The Polar Ocean and Glacial Cycles in
1480 Atmospheric CO 2 Concentration." *Nature* 466. https://doi.org/10.1038/nature09149.
1481 Smith, J M, F P Chavez, and C A Francis. 2014. "Ammonium Uptake by Phytoplankton Regulates Nitrification
1482 in the Sunlit Ocean." *PLoS ONE* 9 (9): 108173. https://doi.org/10.1371/journal.pone.0108173.
1483 Smith, Walker 0., and David M. Nelson. 1990. "Phytoplankton Growth and New Production in the Weddell Sea
1484 Marginal Ice Zone in the Austral Spring and Autumn." *Limnology and Oceanography* 35 (4): 809–21.
1485 https://doi.org/10.4319/lo.1990.35.4.0809.
1486 Smith, Walker O., and Vernon L. Asper. 2001. "The Influence of Phytoplankton Assemblage Composition on
1487 Biogeochemical Characteristics and Cycles in the Southern Ross Sea, Antarctica." *Deep-Sea Research*
1488 *Part I: Oceanographic Research Papers* 48 (1): 137–61. https://doi.org/10.1016/S0967-0637(00)00045-5.
1489 Spiridonov, V. A., E. M. Nöthig, M. Schröder, and A. Wisotzki. 1996. "The Onset of Biological Winter in the
1490 Eastern Weddell Gyre (Antarctica) Planktonic Community." *Journal of Marine Systems* 9 (3–4): 211–30.
1491 https://doi.org/10.1016/S0924-7963(95)00049-6.
1492 Stammerjohn, S., R. Massom, D. Rind, and D. Martinson. 2012. "Regions of Rapid Sea Ice Change: An Inter-
1493 hemispheric Seasonal Comparison." *Geophysical Research Letters* 39: L06501.
1494 Stefels, Jacqueline, and Maria A. Van Leeuwe. 1998. "Effects of Iron and Light Stress on the Biochemical
1495 Composition of Antarctic Phaeocystis Sp. (Prymnesiophyceae). I. Intracellular DMSP Concentrations."
1496 *Journal of Phycology* 34 (3): 486–95. https://doi.org/10.1046/j.1529-8817.1998.340486.x.

https://doi.org/10.5194/bg-2021-122
Preprint. Discussion started: 17 May 2021
© Author(s) 2021. CC BY 4.0 License.

1497 Strickland, John Douglas Hipwell, and Timothy Richard Parsons. 1968. “A Practical Handbook of Seawater
1498 Analysis.” *Bulletin Fisheries Research Board of Canada* 167: 81–86.
1499 Strzepek, Robert F., Maria T. Maldonado, Keith A. Hunter, Russell D. Frew, and Philip W. Boyd. 2011.
1500 “Adaptive Strategies by Southern Ocean Phytoplankton to Lessen Iron Limitation: Uptake of Organically
1501 Complexed Iron and Reduced Cellular Iron Requirements.” *Limnology and Oceanography* 56 (6): 1983–
1502 2002. https://doi.org/10.4319/lo.2011.56.6.1983.
1503 Sunda, W. G., and S. A. Huntsman. 1997. “Interrelated Influence of Iron, Light and Cell Size on Marine
1504 Phytoplankton Growth.” *Nature* 390 (6658): 389–92. https://doi.org/10.1038/37093.
1505 Sunda, William G., and Susan A. Huntsman. 2015. “High Iron Requirement for Growth, Photosynthesis, and
1506 Low-Light Acclimation in the Coastal Cyanobacterium Synechococcus Bacillaris.” *Frontiers in*
1507 *Microbiology2* 6: 561.
1508 Takeda, S. 1998. “Influence of Iron Availability on Nutrient Consumption Ratio.” *Nature* 393 (JUNE): 774–77.
1509 Talley, Lynne D., George L. Pickard, William J. Emery, and James H. Swift. 2011. “Southern Ocean.”
1510 *Descriptive Physical Oceanography*, 437–71. https://doi.org/10.1016/b978-0-7506-4552-2.10013-7.
1511 Taylor, Brad W., Christine F. Keep, Robert O. Hall, Benjamin J. Koch, Lusha M. Tronstad, Alexander S.
1512 Flecker, and Amber J. Ulseth. 2007. “Improving the Fluorometric Ammonium Method: Matrix Effects,
1513 Background Fluorescence, and Standard Additions.” *Journal of the North American Benthological Society*
1514 26 (2): 167–77. https://doi.org/10.1899/0887-3593(2007)26[167:ITFAMM]2.0.CO;2.
1515 Tréguer, Paul, Chris Bowler, Brivaela Moriceau, Stephanie Dutkiewicz, Marion Gehlen, Olivier Aumont, Lucie
1516 Bittner, et al. 2017. “Influence of Diatom Diversity on the Ocean Biological Carbon Pump.” *Nature*
1517 *Geoscience*. https://doi.org/10.1038/s41561-017-0028-x.
1518 Treguer, PJ, and Jacques G. 1992. *Review Dynamics of Nutrients and Phytoplankton, and Fluxes of Carbon,*
1519 *Nitrogen and Silicon in the Antarctic Ocean*. Edited by G Hempel. Springer Berlin Heidelberg.
1520 Vernet, M., W. Geibert, M. Hoppema, P. J. Brown, C. Haas, H. H. Hellmer, W. Jokat, et al. 2019. “The Weddell
1521 Gyre, Southern Ocean: Present Knowledge and Future Challenges.” *Reviews of Geophysics* 57 (3): 623–
1522 708. https://doi.org/10.1029/2018RG000604.
1523 Vogt, M., C. O’Brien, J. Peloquin, V. Schoemann, E. Breton, M. Estrada, J. Gibson, et al. 2012. “Global Marine
1524 Plankton Functional Type Biomass Distributions: ≪I≫Phaeocystis≪/I≫
1525 Spp.” *Earth System Science Data* 4 (1): 107–20. https://doi.org/10.5194/essd-4-107-2012.
1526 Volk, T, and M I Hoffert. 1985. “Ocean Carbon Pumps: Analysis of Relative Strengths and Efficiencies in
1527 Ocean-Driven Atmospheric CO2 Changes.” In *Geophysical Monograph Series*, edited by E T Sundquist
1528 and W. S. Broecker.
1529 Ward, B. B. 1985. “Light and Substrate Concentration Relationships with Marine Ammonium Assimilation and
1530 Oxidation Rates.” *Marine Chemistry* 16 (4): 301–16. https://doi.org/10.1016/0304-4203(85)90052-0.
1531 Ward, B.B. 2005. “Temporal Variability in Nitrification Rates and Related Biogeochemical Factors in Monterey
1532 Bay, California, USA.” *Marine Ecology Progress Series* 292: 97–109.
1533 https://doi.org/10.3354/meps292097.
1534 Weber, Thomas S, and Curtis Deutsch. 2010. “Ocean Nutrient Ratios Governed by Plankton Biogeography.”
1535 https://doi.org/10.1038/nature09403.
1536 Whitworth, Thomas, and Worth D Nowlin. 1987. “Water Masses and Currents of the Southern Ocean at the

https://doi.org/10.5194/bg-2021-122
Preprint. Discussion started: 17 May 2021
© Author(s) 2021. CC BY 4.0 License.

Greenwich Meridian." *JOURNAL OF GEOPHYSICAL RESEARCH*. Vol. 92. https://doi.org/10.1029/JC092iC06p06462.

Yool, Andrew, Adrian P Martin, Camila Fernández, and Darren R Clark. n.d. "The Significance of Nitrification for Oceanic New Production." https://doi.org/10.1038/nature05885.

Zakem, Emily J., Alia Al-Haj, Matthew J. Church, Gert L. Van Dijken, Stephanie Dutkiewicz, Sarah Q. Foster, Robinson W. Fulweiler, Matthew M. Mills, and Michael J. Follows. 2018. "Ecological Control of Nitrite in the Upper Ocean." *Nature Communications* 9 (1). https://doi.org/10.1038/s41467-018-03553-w.